UNIVERSITÀ DEGLI STUDI DI PALERMO

Dottorato di Ricerca in Biomedicina e Neuroscienze

Dipartimento di Biomedicina, Neuroscienze e Diagnostica avanzata (BiND)

SSD BIO/16

GENETIC CHAPERONOPATHIES ASSOCIATED WITH GROUP II CHAPERONIN VARIANTS

LA CANDIDATA

Dott.ssa Federica Scalia

IL COORDINATORE

Chiar.mo Prof. Fabio Bucchieri

IL CO-TUTOR

Dott.ssa Antonella Marino Gammazza

IL TUTOR

Chiar.mo Prof. Francesco Cappello

CICLO XXXII

ANNO DI CONSEGUIMENTO TITOLO 2018/2019

“Usque ad Finem”

List of contents

List of Figures and Images

List of Tables and Graphs

List of Abbreviations

ADP: Adenosine diphosphate
ATP: Adenosine triphosphate
ECM: Extracellular matrix
FITC: Fluorescein isothiocyanate
Hsps: Heat Shock Proteins
IF: Immunofluorescence
PBS: Phosphate Buffered Saline
PCR: Polymerase chain reaction
TRITC: Tetramethylrhodamine

Acknowledgements

I wish to thank all the people who believed in this research project, and not less, in my skills.

My sincere appreciation and gratitude to my supervisor, Prof. Cappello, thank you for your trust, for believing in my ideas, for being my mentor, and for making me grow as a scientific researcher.

My warmest special thanks go to Professors Macario and Conway de Macario for generously giving me all their knowledge, for being my guide during the design of the research plan, for asking the right questions at the right time by stimulating my scientific reasoning skills, and for helping me writing manuscripts.

Nonetheless, I want to thank Prof. Macario and Conway de Macario for their human support and the kindness with which they supported me while I was away from home.

Thanks to Dott. Antonella Marino Gammazza for her precious technical support, for having patiently listened to all my research ideas, for being a friend.

Thanks to Dott. Rosario Barone and Dott. Celeste Caruso Bavisotto for their support, advice and their friendship.

Thanks to Prof. Antonio Giordano and Gianfranco Bellipanni for the internship opportunity at Sbarro institute.

Thanks, for their contribution in this project, to all Professors, Doctors, and Researchers of the Department of Mathematics and Computer Science; of Department of Biological, Chemical and Pharmaceutical Sciences and Technologies; and of Department of Science for the Promotion of Maternal and Child Health.

Finally, I would, of course, like to express my heartfelt thanks to the family of the young patient for the availability; to my family, to my mother and my father, to my friends, Serena, Luca, Morena, Fabrizio, Valeria,

Valentina and Domenico, who have never stopped encouraging me, who have never ceased to give me strength even when we were apart.
To all of you, I wish health and happiness.

Introduction

1. Nervous system

The common characteristic of living organisms is the capacity of interact with the surrounding environment, from which they receive various kind information and stimuli and to which the body modulates suitable responses, attempting to re-establish the initial conditions that the incoming signal had modified (maintenance of homeostasis)[1]. The superior vertebrates also possess a complex of faculties that presides over the so-called psychic acts, as intellectual and affective faculties. The organs intended for all these different functions constitute the nervous system. The nervous system, composed by the central nervous system (CNS), and the peripheral nervous system (PNS), is implicated in the communication with both the external and internal environment of the organism by responding to chemical and physical stimuli (Figure 1)[2].

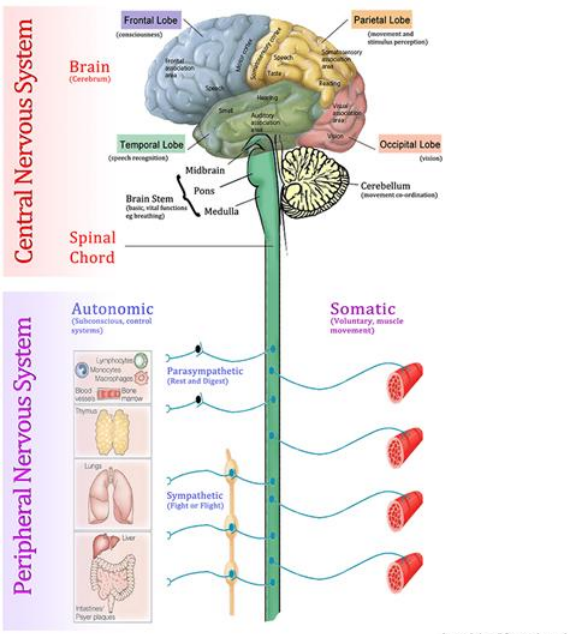

Figure 1

Central and peripheral nervous systems[132]

The main actors of CNS and PNS are neurons and neuroglia cells. They develop from the dorsal ectoderm of the early embryo but different types of them can be distinguished, which are characteristic of the CNS or PNS

(Figure 2). Overall, these cells are responsible for most of the functional features of nervous tissue[2].

1.1 Structure and functions of central nervous system

CNS has the role of processing relevant information, integrating them and producing an efferent response.

It consists of different and communicating anatomical portions. Cranially we found the brain, contained in the skull, made up, in a craniocaudal view, from:

- telencephalon, with the two cerebral hemispheres
- diencephalon
- cephalic trunk, consisting of: midbrain, pons, medulla oblongata
- cerebellum, placed dorsally to the cephalic trunk

Caudally there is the spinal cord, which continues from the cephalic trunk into the vertebral canal.

The neuraxis is essentially composed of two substances: a white substance and a gray substance. In the spinal cord the gray substance is located at the centre of the organ and the white substance at the periphery. In the encephalon the white substance is mostly central and the gray substance appears in the periphery (constituting the cerebral cortex) and partly in depth (constituting for example the thalamic nuclei, the striatum and the nuclei of the cerebellum)[2].

1.2 Structure and functions of peripheral nervous system

PNS is made up of nerves and ganglia (clusters of nerve cells), called spinal nerves and encephalic nerves, which transmit impulses from the afferent stations to the extranervous organs and *vice versa*.

The encephalic and spinal nerves consist of:

- afferent fibers: sensitive, which carry information to the CNS starting from the periphery

- efferent fibers: which carry information to the extranervous organs such as skeletal musculature, smooth, myocardium, glands, starting from the

CNS.

Both types of fibers may have functions:

- somatic: somatic sensitive and somatic motor fibers, linked to voluntary response.
- vegetative: visceral sensory and motor fibers, connected to the involuntary response.

Peripheral nerves may contain both somatic and vegetative fibers (mixed nerves) or just some of them[2].

1.3 Cellular elements of the nervous system: neurons

Neurons are highly specialized cells that receive, process, and transmit information through chemically-mediated electrical signals (Figure 2)[3].

Neurons may differ from each other in specialization and morphology, however they share some features. Mainly these have the function of communicating with other types of cells. When the nerve impulses travel along the axon (an elongated tubular structure that extends from the cell body and ends in proximity to other cells; axons can vary in length, ranging from less than a millimetre to longer than a metre) in the form of an action potential, it arrives in the specialized structure called synapse, made up of presynaptic membrane of axon terminal, a synaptic cleft, and a postsynaptic membrane of a neuron's dendrite (projections that increase the surface area available to receive signals from other neurons), soma, or less commonly, axon. Following the arrival of action potential the vesicles at the axon terminal, which contain neurotransmitters or neuromodulators, release their content by exocytosis in synaptic cleft. The chemical transmitters travel across the synaptic cleft to reach receptors on the postsynaptic cell. This is the classic description of the synapse of vertebrates and invertebrates, supported by the Ramòn y Cajal neuron doctrine and by much of the scientific world. However, to this description it is necessary to combine the results which several studies and new technology applications, such as electron microscopy, have pointed out. They, instead, support the existence within CNS of new synapses, called

mix synapses and synapses à distance, where the axon and the dendrites appear to be exchanging their roles. This would open the door to a reform of the classical doctrine on neuron[3].

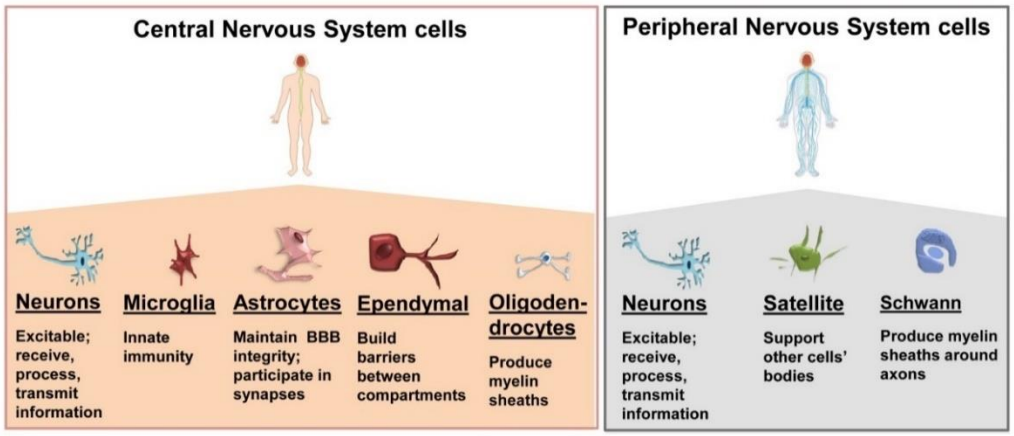

Figure 2

Cellular components of the central and peripheral nervous system[3]

1.4 Cellular elements of the nervous system: glial cells

Over the years it has always been thought that glial cells were cells with poor activity, and that their only function was to provide support and nutrition to the neurons, form myelin, and, by insulating axons, speed up electrical communication[3]. Also, the term glia from the ancient Greek word "glía" meaning "glue" in English, suggested a rather "stuck" function of this type of cell. Despite it has been thought that glia do not participate directly in synaptic interactions and electrical signalling, emerging findings suggests that glia, particularly astrocytes, play a role in the formation of synapses and in modulating synaptic function through bidirectional communication with neurons, both during development and in adulthood[4].

The number of glial cells compared to the number of neurons has also been the subject of discussion for many years. It was thought that glial cells were a larger proportion. Recent studies show that the number of glial cells is very close to the number of neurons in the human cortex. A distinction in terms of a cell type amount rather than another can occur in specific areas of the brain[5].

1.4.1 Neuroglia of the CNS

Neuroglia of the CNS can be divided into macroglia and microglia (Figure 2). Oligodendrocytes, astrocytes, and ependymoglial cells belong to the macroglia which originate from the ectoderm, while cells derive from the yolk sac represent the microglial. They are found in the CNS during early embryonic development[6].

Different subclasses of oligodendrocytes (OLGs) derived from multiple sources are in spinal cord and brain (Figure 2). The role of OLGs is provide a lipid-based insulation and, thus, boosting the speed at which the action potential can get around in the axon[3].

The NG2-glia/oligodendrocyte cells are particular oligodendrocyte characterized by the presence on their surface of chondroitin sulfate proteoglycan. Although their function is not yet fully known, they are considered an independent glial population. Nowadays it has been discovered that NG2-glia 1) act in maintaining the physiological and homeostatic conditions of the nervous tissue generating mature myelinating oligodendrocytes, 2) it cooperate in synapses building with neurons of the hippocampus and presumably in other parts of the brain. Notably, NG2-glial cells have the ability to receive signals without creating or propagating action potentials[7].

The astrocytes, called like this by their star-like shape of cytoplasmic processes, are supportive glial cells in neural tissue[8].

The maintenance of a healthy CNS can be attributed to the role that astrocytes have within it: the maintenance of water and ion homeostasis and blood–brain barrier (BBB) integrity; the contribution in tripartite synapses, where astrocytes are active actors. Astrocytes can inhibit or enhance overall levels of neuronal activity by releasing neurotransmitters[3]. While, in past years, there has been talk of two types of astrocytic cells, today are recognized up to four major classes of GFAP+ astrocytes in the human brain: in layers I and II of the cortex there are interlaminar astrocytes; in layers III and IV can be found protoplasmic astrocytes; in

layers V and VI are located astrocytes in varicose projections; in white matter reside fibrous astrocytes[3].

From the neuroepithelium derived the CNS macroglia. It is constituted by ependymoglial cells located in the interface between the brain parenchyma and the cavity of the ventricles in the CNS, and in the central canal of the spinal cord. These have various shapes, from cuboidal to columnar with cilia and microvilli on the apical surfaces since their role is to maintain absorbance and circulation of cerebral spinal fluid (CSF)[3].

Within ependymoglial cells it is possible to distinguish 1) ependymocytes, which make contact with the basal lamina labyrinths (remnants of embryonic blood vessels) and with the ventricles where they contribute to the CSF movement, 2) choroid plexus epithelial cells, which secrete CSF, 3) tanycytes, highly specialized ependymal cells that form a blood–CSF barrier and blood–CSF homeostasis[3].

Unlike previous, microglial cells originate from mesodermal hematopoietic cells that in mammals come from the yolk sac. Notwithstanding the blood cells, microglial cells play a role as innate immunity of the CNS acting as unique tissue-resident macrophages involved in immune reactions (defending against bacterial and viral infections) and inflammatory diseases (Figure 2). Furthermore, they have self-renewal potential[3].

Attractive are the additional roles of microglial cells in 1) the maturation of neural circuits by their “synaptic pruning” function[9], 2) maintain mature neurons by the release of brain-derived neurotrophic factor (BDNF), 3) mediate synapses, 4) and remove myelin debris by phagocytosis[3]. Microglial cells are the inspectors of the microenvironment, exploring the cerebral parenchyma with their processes and moving bodies[10].

1.4.2 Neuroglia of the PNS

PNS is composed by two types of neuroglia: cells that make myelin sheath around axons, the Schwann cells (SCs); and cells checking nutrient and neurotransmitter levels in ganglia, the satellite glial cells (Figure 2)[3].

SCs are play a role in PNS as the oligodendrocytes in CNS do. They are among the main actors in the neuromuscular synapse formation, promoting the efficient and energy low-cost propagation of axon potentials via saltatory conduction by maintaining internodal—each myelin segment is flanked by unmyelinated nodes of Ranvier–myelin sheath thickness and length relative to the diameter of the corresponding axon[3]. Furthermore, the homeostasis of synapses is under the control of terminal Schwann cells (tSCs, also called non-myelinating SCs or perisynaptic SCs) which have a role in “synapse elimination” and synaptic pruning during development and, throughout adult life, but also trigger the regeneration of injured peripheral motor axons[11].

Satellite glial cells (SGCs) line the sensory dorsal root ganglia of the spinal cord. SGCs express glutamine synthetase and various neurotransmitter transporters, they go checking into microenvironment and impact synaptic transmission. Thus, they are similar to astrocytes[12].

1.5 Reception and interpretation of information

The ability of the central nervous system to receive information is due to the presence of specific peripheral receptors which after specific stimulation:

- transmit the message to afferent fibers
- the message reaches the central nervous system
- effector responses are realized with different levels of complexity.

The simplest answer is the one that is realized through the *reflex arcs* where an afferent fiber directly activates an efferent neuron without passing into the brain, but doing synapse in the spinal cord. The answer coming directly into the efferent fiber in the periphery, determines an almost immediate response.

The most complex answers involve the assistance of higher centers located in the brain, to which the message coming from ascending fibers is revised and so the sensations that come from the periphery become conscious, hence perceived[2].

The interpretation of the nervous message carried out by the higher centers is based on the type of receptors that collected the stimulus. Although different sensory pathways converge in the same nuclei before reaching the encephalon, is always maintained a certain anatomical diversity between the ways that carry different types of sensitivity. This anatomical diversity allowed the distinction of specialized areas of the cerebral cortex (Brodmann area) for a precise sensitivity[1].

There are several types of receptors capable of receiving different types of stimuli / sensitivity.

The ascending pathways that carry precise information to the higher centers also have the task of recognizing the type of stimulus and the location in which it occurred.

The responses to the different types of stimuli are instead implemented by descending nerve pathways, which regulate the contraction of skeletal muscles, smooth muscles and gland activity.

Smooth muscles and glands are governed by the vegetative or autonomous nervous system, which stands out in:

- orthosympathetic: generates an increase in activity
- parasympathetic: it restores the functioning of the visceral organs to standard values[2].

1.6 Neuromuscular Junction: the “nervous side”

The neuromuscular synapse is a typical synapse formed between a spinal motor neuron and a skeletal muscle cell. The synaptic transmission at the skeletal neuromuscular junction is very similar to the synaptic transmission that occurs in the central nervous system.

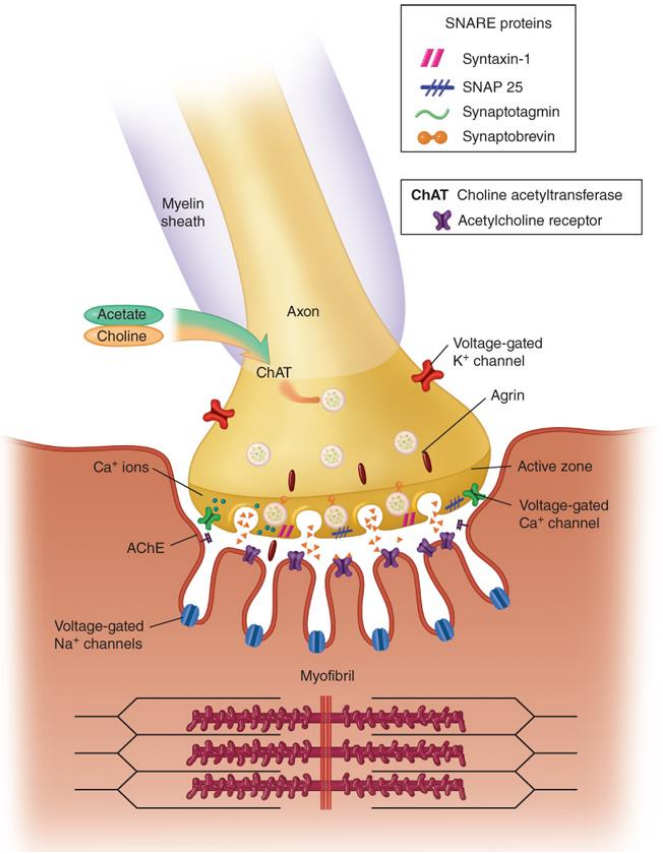

Figure 3

Neuromuscular junction (source : presynaptic terminal of motor neuron and a muscle fiber form the chemical synapse. Calcium ions enter into neuron trough voltage-gated calcium channels (green) activated by action potential transmission. Synaptic vesicles (spheres inside motor neuron terminal) merge with neuron cell membrane and acethylcoline neurotransmitter (substance within spheres) is released into synaptic cleft. Acetylcoline (orange triangles) binds to nicotin acetylcoline receptors (lila) on the muscle fiber cell membrane. This binding allow the depolarization of the muscle fiber and results in sarcomeres contraction.[13]

Cell bodies of motor neurons are located in the ventral horn of the spinal cord, seeping out of the spinal cord the motor neurons reach and innervate the skeletal muscle fibers with the terminal region of the axon. It generates a meticulous processes throughout skeletal muscle cells. This particular synapse is called motor endplate because of its specific structure. Some features of neuromuscular junction (Figure 3) are 1) a distinct separation between the presynaptic (neurons) and the postsynaptic (muscle) membrane. The space between the two membranes is the synaptic cleft where neurotransmitter is released and travels to carry information to muscle fibers; 2) an high density of vesicles containing neurotransmitter and of mitochondria; 3) an high density of specialized

receptors in postsynaptic membrane to ensure the binding of neurotransmitters to receptors (Figure 3)[13] .

2. Rare neurodegenerative disease: leukodystrophies

The history of leukodystrophies extends over a century or so, with many studies on the various aspects of these serious conditions but the major problem of the classification of cases within a coherent system still remains unresolved [14].

The term leukodystrophy was coined in 1928 as the condition Metachromatic Leukodystrophy (MLD) was described[15]. It comes from the Greek leuko (white), dys (abnormal), and trophy (growth), and intends to define deficient growth or development of white matter. Later, in the 1980's the term was associated with defects in myelin. This concept is valid still today and is a little different than that indicated by the word leukoencephalopathy: a more encompassing term that includes genetic and acquired brain white matter disorders[14].

By the end of the 1980's and early 1990's efforts were made to find genes associated with leukodystrophies. Thus were identified a gene encoding proteolipid protein (PLP, PLP1) associated with Pelizaeus–Merzbacher disease (PMD)[16]; the arylsulfatase A gene for MLD[17]; the gene encoding the aspartoacylase for Canavan disease[18]; the gene encoding the galactosylceramidase for Krabbe disease[19]; and the ATP-binding cassette subfamily D member 1 for X-linked adrenoleukodystrophy[20]. By 2010 gene defects in the majority of leukodystrophy cases had been identified. However, about half of patients could not be properly diagnosed or classified, and it was observed that over the years the number of new cases with novel genetic defects increased considerably[21].

Whole exome sequencing (WES) helped in the study of hereditary diffuse leukoencephalopathy with spheroids" (HDLS)[22]. Later on, WES revealed for HDLS, dominant mutations in Colony Stimulating Factor 1 Receptor[23]. Soon thereafter, recessive mutations were found in mitochondrial glutamyl-tRNA synthetase in patients with

"leukoencephalopathy with thalamus and brainstem involvement and high lactate"[24], and dominant de novo mutations were revealed in Tubulin Beta 4A Class IVa in the sporadic disease "hypomyelination with atrophy of basal ganglia and cerebellum"[25].

WES proved very useful for discovering gene variants associated with many Mendelian abnormalities in the period 2011-2016[14]. However, many cases still remain undiagnosed or not properly characterized and, therefore, are not counted or classified in any group of neurodegenerative diseases. Many years ago and even up to 2015, nearly half of all patients in whom neuroimaging studies indicate a defect in white matter and whose clinical manifestations suggest a genetic etiology are undiagnosed[26,27]. This could be the result of a limitation in the classification criteria. For instance, the definition currently shared by the scientific community does not discriminate cases on the basis of which organelle is involved in each disease. Furthermore, the extant definition does not point specifically to a subcellular compartment, despite the fact that many pathologies involve preferentially one of the various cell compartments, and despite the fact that clinical cases are usually characterized by the dysfunction of the synthesis and degradation of the myelin sheath.

During my PhD, in addition to studying specific mutations, I have worked very hard to propose to consider the participation of molecular chaperones (many of which are heat-shock proteins, Hsps in short) in the mechanism of disease as a way to sort out various leukodystrophies. I propose a pathogenetic view based on the role of molecular chaperones that, I hope, will provide a rational scaffold to organize information on leukodystrophies and to classify patients into distinct categories. This in turn, will help in differential diagnosis of new patients and in deciding on specific therapeutic strategies using chaperones as target or agents (section 5. Chaperonotherapy).

3. Molecular chaperones

The molecular chaperones are evolutionarily conserved proteins, present in the cells of all organisms, eukaryotes and prokaryotes. They are

essential for the control of protein homeostasis and the maintenance of correct and functional conformation of proteins and of nascent polypeptides, preventing their aggregation and misfolding [28]. Actually, they have many other roles unrelated to proteins folding and depending on the organ status (physiological or pathological) where they lie. Molecular chaperones also assist protein refolding and translocation through membranes, occur during proteins repair and degradation, and dissolve protein aggregates. Furthermore, several chaperons are heat shock proteins. The term heat shock protein (Hsp) indicate that protein expression can be induced by temperature elevation. As a matter of fact, these genes respond to different types of environmental stressors, such as disease states, hypoxia, ischemia, hyperoxia, exposure to toxic and carcinogenic factors [29]. Nevertheless, not all Hsps are component of chaperoning system. It can be said that not all chaperones are Hsps, and not all Hsps are chaperones. To Hsps have also been assigned other functions, not necessarily related to homeostasis of proteins, such as the regulation of gene expression and DNA replication [30], cell differentiation [31], signal transduction [32] and inflammatory response [33], the process of carcinogenesis [34], senescence [35] and cell apoptosis [36].

Traditionally, molecular chaperones are regarded as intracellular proteins, with localization in the cytoplasm, mitochondria, endoplasmic reticulum, peroxisomes and in the nucleus. However, their presence has been demonstrated in several sites in the extracellular environment, indeed, can be released from cells in a variety of circumstances and interact with adjacent cells or in some cases enter the bloodstream and are present in fluids such as blood, lymph and cerebrospinal fluids [37].

The Hsp-chaperones are generally grouped into classes, based on their peptide sequence homology, structure, or in the molecular weight. Therefore, it is possible to distinguish: Hsps with high molecular weight (with a mass greater than or equal to 100 kD), Hsp90 (with mass between the 81 and 99 kD), Hsp70 (with a molecular weight between 65 and 80 kD), Hsp60 (between 55 and 64 kDa), Hsp40 (between 35 and 54 kD) and

small Hsps (having a mass less than or equal to 34 kD). Each of these families includes various isoforms (Table 1) [38].

Name	***HUGO Name*** [39]	***Old Name***	***Mass (kDa)***	***Main functions***
Super-heavy	DNAJC28	Sacsin	≥200	Prevents protein aggregation, helps protein folding.
Heavy	HSPH	High MW; Hsp100	100-199	Prevents protein aggregation, helps protein folding.
Hsp90	HSPC	HSP86, HSP89A,HSP90A, HSP90N, HSPC1, HSPCA, LAP2, FLJ31884	81–99	Protein folding, cytoprotection; intracellular signalling (e.g., steroid receptor); cell-cycle control.
Hsp70	HSPA	Chaperones, DnaK	65–80	Prevents protein aggregation, protein folding, cytoprotection and anti-apoptotic function.
Hsp60	HSPD1	Chaperonins (groups I and II), Cpn60 and CCT	55–64 35–54	Prevention of protein aggregation, protein folding, cytoprotection, macrophage activator possibly through Toll-like receptor.
Hsp40	DNAJA	DnaJ	35-54	Protein folding and refolding together with Hsp70/Hsc70.
Small Hsp	HSPE1	sHsp, alpha-crystallins, Hsp10	≤34	Protein folding together with Hsp60; modulation

		of immune system.
Other	Proteases, isomerases, AAA+ proteins (e.g., paraplegin or SPG7, spastin or SPG4); α-hemoglobin-stabilizing protein	Various

Table 1

Subpopulations of Hsp chaperones (modified from Macario and colleagues, 2010 [35])

During my PhD I investigated the role of two components of chaperoning system, Hsp60 and CCT proteins.

4. Chaperonins

The chaperonins are evolutionary-conserved, indeed, they are essential in all sequenced organisms. The chaperonins are subdivided into two families, termed the group I and group II chaperonins.

4.1 Hsp60, molecular chaperonin of group I

The Hsp60 is a ubiquitous protein presents both in eukaryotes and prokaryotes, including pathogens [40]. The human Hsp60 is a mitochondrial chaperonin phylogenetically related to the bacterial protein GroEL [41]. This chaperonin complex is composed by two rings made up of seven identical subunits each. The monomer or subunit is about 60 kDa and tends to associate in rings, which in turn pair to form heptadecamers. Each monomer is constituted by three domains: an apical domain, which represents the binding site for polypeptides, an equatorial domain, which contains the binding site of ATP/ADP and an intermediate domain, which acts as a connector of the other domains (Figure 3) [42,43].

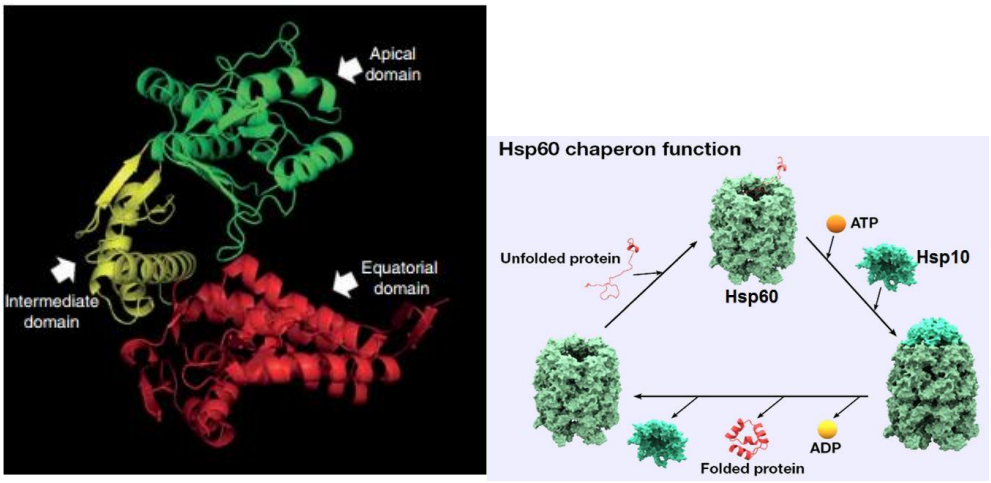

Figure 4

Hsp60 monomer structure showing its three structural domains: apical in green, intermediate in yellow and equatorial in red. (from Cappello and colleagues, 2014 [43]). Hsp60 works in cooperation with Hsp10, its co-chaperonin, to assist protein folding of unfolded mitochondrial proteins by an ATP-dependent mechanism.

Hsp60 is a stress-induced protein, not constitutively expressed, classically considered an intracellular chaperone. Under specific conditions it takes part to chaperoning system and during folding process it works with Hsp10, its co-chaperone. Being responsible for the protection of cells against all stressors is essential for cell survival [44]. Hsp60 is tipically localized in the mitochondria matrix, however, several studies have shown its presence in extra-mitochondrial sites, such as the cytosol and plasma membrane. Furthermore, recent studies demonstrate that when Hsp60 is localized in extracellular environment and bloodstream, it can interact with immune system cells stimulating cells at distant site in the body. For this cause, Hsp60 was called also a *chaperokine*. Hsp60 may induce maturation of human monocyte-derived dendritic cells and T cell polarization and may trigger the monocyte and macrophage cells to synthetize pro-inflammatory cytokines, such as TNF-α, lL-12 and IL-15 [45,46].

It has been supposed that the immunological characteristics of Hsp60 are due to its high degree of homology with prokaryotic Hsp60, inducing autoimmunity as a failure of the mechanism of self-, not self-

discrimination[41]; it acts a role in maintenance of inflammation in autoimmune [47] and chronic inflammatory disease [48].

4.2 CCT, molecular chaperonin of group II

CCT group II chaperonins are found in archaea and the eukaryotic cytosol. They also consist of two stacked rings, each composed of eight 50–60 kDa subunits, but do not have an obligate co-chaperone in the same manner as the group I chaperonins[49]. Rather, they contain a built-in lid that closes the folding chamber and are thus competent to fold substrates in vitro without the assistance of accessory proteins. This should not be taken to mean that the group IIs function in isolation in the cell. On the contrary, the group II chaperonins appear to be at the heart of a complex network of co-chaperones. Notable examples include the hexameric prefoldin complex which is often thought to bind to and prevent aggregation of unfolded substrates before handing them off to the chaperonin and the phosducin-like proteins which have been shown to enhance CCT-mediated folding of several substrates[50].

The eukaryotic group II chaperonin, which is known as TCP1-complex/TRiC/CCT (CCT hereafter), differs from its simpler archaeal homologues in that it is composed of 8 paralogous subunits. Most notably, CCT is absolutely required for folding many essential proteins, including cytoskeletal proteins like tubulin and actin as well as cell cycle regulators such as CDC20, CDH1. It has been estimated that as much as 10% of cytosolic proteins interact with the eukaryotic chaperonin CCT along their folding trajectory[51]. For this reason, contrary to Hsp60, CCT is constitutively expressed from almost all cells type.

Also subunits of group II chaperonins share a similar basic structural pattern with subunit of group I and consist of three domains: a) an apical domain which is related to the binding of substrate, b) equatorial domain, and function related to ATP binding, c) hinge domain which enables the connection between rests of the two domains[50].

5. Chaperonopathies

Disorders associated either with defective chaperones, or else with protein molecules whose primary sequences resemble those of chaperones have been identified since many years ago[28,52,53,54]. These pathologic conditions constitute a subset of the proteinopathies and are termed chaperonopathies[28].

Mutations, genetic or acquired, can affect one or more of the specialized functions of the entire molecule, of the subunit, or of the subunit domains of a molecular chaperone. Upon this, the pathologic/clinical manifestations of a chaperonopathy depend[28]. It is important to state, that functional domains do not necessarily reside in a continuous stretch of amino acids, but, functional domains can also be formed by non-contiguous segments of the protein who join subsequent to folding into a tertiary structure. A mutation affecting a domain could be in an unsuspected position in the primary structure. So far we have been talking about structural chaperonopathies, but the defect could be regulatory if the expression of a chaperone is increased or decreased[53,55,54].

Among structural chaperonopathies there are also post-translational defects due to either RNA truncation, or else protein oxidation, glycation, or other post-translational modifications[54]. These are mostly acquired and occur predominantly in adults and aged individuals.

Mutations on Hsps themselves can lead to chaperonopathies that also are mostly associated with accumulation of protein aggregates. Among the first chaperonopathies found were those due to mutations in members the small Hsp family. Later, members of the chaperonins and DNAJ families as well as chaperone cofactors (e.g., in BAG3, a Hsp70-NEF) have been found defective and causing inheritable chaperonopathies.

Clinically, these genetic chaperonopathies can be sorted into various categories, for instance neuropathies (e.g., hereditary spastic

paraplegia, motor neuropathy, distal hereditary motor neuropathy), myopathies (e.g., dilated cardiomyopathy, leukodystrophy, desmin-related myopathy, mitochondrial myopathy, muscular dystrophy) or retina- and eye lens-related diseases (e.g., congenital cataracts)[28]. A classification of chaperonopathies based on their distinctive features are shown in Table 2.

Types of chaperonopathies	***Causes***	***Condition***
Genetic	Gene mutation, Hereditary, Congenital	Motor neuropathies, ataxias, Bardet-Bield and Williams syndromes; cardiomyopathies; endoplasmic reticulum pathologies [35,56]
Acquired	By defect and By excess	Aging due to pathological post-translational modifications, such as oxidation, phosphorylation, acetylation, or glycation [35,56]
	By mistake or collaborationism	Autoimmune and inflammatory disease, cancer [35,56]

Table 2

Types of chaperonopathies and main features

5.1 Involvement of chaperonins in neurodegenerative diseases: Hsp60 and CCT

Pelizaeus-Merzbacher-like disease (PMLD [MIM 608804 and MIM 260600]), which can be considered the prototype of primary hypomyelinating leukodystrophies (HMLs or HMDs), is an autosomal-recessive disorder clinically indistinguishable from PMD but in which PLP defects are not found[57].

Mutations in the GJA12 gene encoding the gap junction protein connexin 47 (Cx47) have been identified as causing PMLD[58]. Nevertheless, according to recent data, GJA12 defects account for less than 10% of PMLD cases[59], and there are many patients of both genders who suffer from PMLD, and who carry neither PLP nor GJA12 mutations, suggesting

the involvement of additional, as-yet-unidentified genetic defects that may also cause perturbation of normal myelin genesis.

Through technological advances, including next-generation sequencing technology, defects in ten different somatic genes have been identified that are associated with HMDs[60].

Mutations of the gene HSPD1 have been found associated with disease[61]. Its protein product, the mitochondrial chaperonin Hsp60 (designated HSPD1in humans) participates in the folding and assembly of newly synthesized polypeptides inside the mitochondria[62]. As of now, the HSPD1-associated diseases are the mitochondrial Hsp60 chaperonopathy (MitCHAP-60 disease), spastic paraplegia 13 (SPG13), and hypomyelinating leukodystrophy 4 (HLD4)[57].

Hereditary spastic paraplegia (HSP or SPG) is a heterogeneous disease characterized by gait disturbance caused by spasticity and weakness of the lower limbs[63]. Age of onset is typically in the third or fourth decade of life. The disease is traditionally classified into “pure” and “complicated” forms depending on the presence of additional neurological or systemic abnormalities. The major pathological feature is a progressive degeneration of the longest axons of the descending (corticospinal) and the ascending (sensory) tracts in the spinal cord[64]. The HSPs are among the most genetically diverse neurologic disorders, with well over 70 distinct genetic loci, for which about 60 mutated genes have already been identified[65]. Judging from known functions of the proteins encoded by the mutated genes, two major pathogenetic mechanisms have been envisaged: one affecting axonal trafficking[66] and one affecting mitochondrial function and endurance[67]. However, because mitochondria use the axonal transportation systems and transportation requires energy, both mechanisms are not mutually exclusive and may even be complementary.

Previously, analyzing a French family with autosomal dominant pure hereditary SPG13, it was detected heterozygosity for a mutation (c.292G > C; p.Val98Ile) in the HSPD1 gene, which encodes the mitochondrial

Hsp60 chaperonin[68]. The mutation co-segregated with the disease in the large pedigree.

To shed light on the molecular mechanisms underlying spastic paraplegia due to the Hsp60-(p.Val98Ile) mutation, the corresponding mutant protein was expressed and purified and its properties and ability to assist folding of a test protein in vitro was analyzed[69]. In addition, it was engineered a flexible E. coli experimental system that allowed to monitor various phenotypes in E. coli and to study potential dominant negative effects of co-expression of mutant Hsp60-(p.Val98Ile) and wild-type Hsp60[69]. It was observed that the Val98Ile mutation affects the ATPase activity and results in a dramatically decreased folding activity of complexes consisting of the mutant subunits only. However, in contrast to an artificially constructed ATPase mutant, the Val98Ile mutation exerts no salient dominant negative effect when co-expressed with wild-type Hsp60. Because no effect of the mutations on complex assembly was observed, it is assumed that heptameric complexes with all possible combinations and arrangements of subunits are formed. Incorporation of only one or two ATPase mutant subunits has a dramatic effect; whereas complexes composed of Hsp60-(p.Val98Ile) and wild-type Hsp60 subunits appear to possess activity, although reduced in comparison with the wild-type complex.

A missense mutation, p.Gln461Glu, in the HSPD1 gene in one out of 23 Danish SPG patients has been identified[70].

The causative nature of this mutation is uncertain because two siblings carrying this mutation were asymptomatic. However, through a sophisticated genetic complementation assay it has been established that E. coli cells expressing Hsp60-p.Gln461Glu show a mild functional impairment; this variation may be disease-associated with reduced penetrance.

E. coli mutant cells lacking the groES-groEL genes but complemented with the human Hsp10 and Hsp60 genes display reduced growth, compared to cells complemented by the wild type Hsp60. These results suggest that the functions of the Gln461Glu mutant protein are mildly compromised and

are consistent with it being associated with SPG but having a low penetrance. The p.Val98Ile Hsp60 mutant previously associated with a highly penetrant late-onset SPG in a large family was shown to be more severely functionally impaired. Reduced penetrance of autosomal dominant SPG has been reported in association with mutations in SPG3A (encoding atlastin)[71] and in SPG4 (encoding spastin)[72]: approximately 12% of SPG cases without a family history of SPG were found to be due to heterozygosity for mutations in SPG4. It is possible that the Gln461Glu missense mutation previously described[70] is unable to cause SPG by itself but instead causes SPG in combination with other genetic or environmental risk factors. By analogy to the resolved structure of the homologous E. coli GroEL protein, the spastic paraplegia associated amino acid changes in HSP60, p.Gln461Glu and p.Val98Ile, are likely situated in the same region of the Hsp60 structure and could compromise chaperone function in a similar way by interfering with conformational changes that occur in this specific region. Also bioinformatics prediction of the effects of the variations, using the PolyPhen-2 tool (Adzhubei et al., 2010), predicts damaging effects for the Hsp60-p.Val98Ile and Hsp60-Gln461Glu variations, but benign for the Hsp60-p.Asp29Gly for which a clear disease relationship has been established.

An autosomal-recessive hypomyelinating leukodystrophy caused by a missense mutation in the mitochondrial Hsp60 chaperonin was described, which was designated MitCHAP-60 disease or HLD4[57].The ten patients studied exhibited the following shared cardinal features: (1) rotatory nystagmus, which was the presenting symptom in most patients; (2) progressive spastic paraplegia within the first months of life, followed by a variable rate of neurological deterioration and regression; (3) severe motor impairment, with none of the affected children ever gaining normal head control; (4) profound mental retardation; and (5) hypomyelinating leukodystrophy as evidenced by brain magnetic resonance imaging (MRI).

The use of homozygosity mapping and then mutation analysis of candidate genes within the linked locus on 2q32.3-q33.1 enabled to

pinpoint a homozygous missense mutation (Asp29Gly) in HSPD1, as responsible for MitCHAP-60 disease[57]. Several findings support the causative role of the Asp29Gly mutation in the pathogenesis of MitCHAP-60 disease. These include (1) consistent segregation of the mutation with the disease-associated phenotype in all investigated family members; (2) the absence of the mutation in a large number of ethnically matched controls; (3) the high degree of conservation of the Asp29 residue across Hsp60 homologs of various nonhuman species, from vertebrates to bacteria, suggesting its functional importance; and (4) the E. coli complementation-assay results, which demonstrate the markedly reduced ability of the Hsp60 mutant gene to support E. coli survival at all temperatures, especially at the highest tested. Taken together, all these findings strongly suggest that the homozygous state of the g.1512A/G mutation resulting in the HSPD1 Asp29Gly mutation compromises the protein functions and is responsible for the severe phenotype of MitCHAP-60 disease[57].

The fact that E. coli survival was not completely abolished by the Asp29Gly-Hsp60 variant suggests that the amino acid substitution may exert a less severe effect on Hsp60 function, as compared to the previously described HSP60-Val98Ile variant causing SPG13. This result is not surprising, given the fact that all heterozygous carriers of the Asp29Gly mutation are asymptomatic, with some of the carriers reaching their ninth decade of life, indicating that a single Asp29Gly mutant allele does not significantly impair overall mitochondrial Hsp60 activity[57]. Of special interest are the potential mechanisms by which different mutations in HSPD1 may lead to such dramatic differences in both the pattern of inheritance and the disease phenotype between SPG13 and MitCHAP-60.

Consistent with the functional analyses of the aforementioned study, different patterns of inheritance of MitCHAP-60 and SPG13 may thus be explained in the following way: the Asp29Gly mutation, which exerts a relatively mild effect on Hsp60 function, only manifests in the homozygous state, whereas the Val98Ile mutation, having a more severe effect on

Hsp60 activity, produces a phenotype in the heterozygous state. Nevertheless, homozygosity for the mild mutation causes a more severe phenotype than heterozygosity for the severe one[57].

Effects of expressing the SPG13- and MitCHap60-associated mutant proteins on mitochondrial morphology and dynamics have been assessed in Cos-7 cells transfected with cDNAs encoding the disease-associated mutant proteins[75,76]. Cos-7 cells expressing either the mutant variants HSP60-p.Asp29Gly, or HSP60-p.Val98Ile, or HSP60-p.Gln461Glu exhibited increased number of mitochondria, short mitochondria, and decreased mitochondrial membrane, whereas Cos-7 cells transfected with wild type HSP60 cDNA did not. These studies indicate that the mutated proteins interferes with the action of the endogenous counterparts wild-type proteins.

Although, there is considerable information on the clinical manifestations of these chaperonopathies, and on the inheritance patterns of the genetic cases that have been studied in detail, the impact of these mutations on the functions of HSP60 has not been fully clarified[75]. This scarcity of knowledge is mostly due to the lack of appropriate animal models that mimic closely the human molecular, cellular, and histological characteristics.

5.2 Mutation in the CCT5 Subunit Gene

It is reported instead that His147Arg point mutation in cct5 gene, encoding the subunit 5 of CCT complex cause a disease characterized by hypomyelination in the posterior tract of the spinal cord. Clinical and pathological manifestations are characteristic of a distant sensory neuropathy (Table 9). Four patients harbor the His147Arg mutation in homozygosis. The amino acid change occurs within the equatorial domain of the CCT5 subunit, therefore this suggests that the chaperoning ability to bind and hydrolyze ATP is impaired. It was confirmed by several studies on archaeal model in which the His147Arg mutation results in an instability of hexadecamers and ATPase activity affected[76]. Other studies using

recombinant human CCT5 confirm the data[77,78].

CCT interacts mainly with actin and tubulin but its interactome involves 5%–10% of the mammalian proteome[79]. Therefore, if myelin proteins are client proteins of CCT complex not yet identified, mutations in CCT5 subunit can impair their folding or transport throughout cytoskeleton[75].

6. Zebrafish as a *in vivo* model to study Chaperonopathies

To study human chaperonopathies a prokaryotic model has been used to explain some molecular implications of CCT 5 mutated subunit causing chaperonopathy[76]. Zebrafish has proved to be a good model for the study of both genetic[80] and acquired[80] diseases resulting in chaperones defects, and generally, it is still one of the best animal models to study humans diseases[81].

The advantageous features of this fish, originally found in the south-east of the Himalayas are many and make it a good model to study neurodegenerative disease: its external fertilization; the fast growth; the transparency of the embryo and, furthermore, it is manageable with different embryological, biochemical, molecular techniques. Mutagenesis by irradiation was firstly used on it[82], later, zebrafish was used for N-ethyl-N-nitrosourea (ENU) mutagenesis and mutagenesis screens[83]. The most important discovery was that many genes and biological mechanisms were evolutionarily conserved from the zebrafish to humans. That made this animal model accepted by scientific community. To date, zebrafish is used for modeling of human diseases, knocking-down genes via morpholinos[84], or creating transgenic fish[85] applying the more recently developed reverse genetic techniques[86,87]. Not only at the genome level but also at the cellular and organism level, zebrafish is very close to human species. Studies on angiogenesis, cardiac development, and regeneration, on the function of the nervous system, and nociception, on cancer and metabolic diseases successfully demonstrate this similarity[88,89,90]. This was definitely confirmed in 2013, once the whole zebrafish genome was completely sequenced[91]. Despite its peculiar

characteristics, like the ability to regenerate nerves, fins, and heart tissue, zebrafish remains a hight-potential animal model.

6.1 Heat-Shock Proteins and Chaperone Genes in Zebrafish

Molecular and genetic studies confirm that in zebrafish there are many genes of the chaperoning system which are homologs to those present in humans (Table 3).

Name	Genes	Mutants	Transcripts	Pseudogenes
hsp	97	44	61	0
chaperone	34	19	0	0
cct	10	7	8	0

Table 3

Source: http://zfin.org/; ZFIN: The Zebrafish Model Organism Database[92]

For these reasons zebrafish offers the possibility of modeling human genetic chaperonopathies. Despite the environment in which zebrafish lives, it is quite different from that in which most mammals live, they express heat shock factors 1 and 2 (HSF1 and 2) and therefore they are capable of responding to heat shock or other stressful stimuli[93]. Furthermore, many of these genes are expressed during zebrafish embryogenesis. Some of the molecular chaperones genes studied in zebrafish are individually discussed below.

Aims

As discussed, genetic chaperonopathies manifest themselves from very early in life. Chaperonopathies related to neurodegenerative disorders discussed in “Introduction” section are a heterogeneous group of disorders which affect one or more of the various physiological systems, for example the nervous system. This heterogeneity is due, in particular, to the not fully known molecular activity, which every single molecular chaperone has within a specific tissue. My general questions about them were 1) why a mutation on a molecular chaperone that is expressed by most, if not all cytotypes, seems to affect the functioning of a single physiological system? 2) why do different mutations on the same molecular chaperone cause apparently different pathologies especially in terms of clinical manifestations?

This heterogeneity limits the research approach on diseases, which now is conducted towards every single mutation without being able to generalize a unique molecular process.

I spent the first 18 months of my Ph.D. project at the SBARRO Department of Temple University in Philadelphia to study the V98I mutation on chaperone Hsp60 causing hereditary spastic paraplegia (SPG13). For a better understanding of the associated diseases, it would be highly beneficial to examine the impact of mutant chaperone genes during development, starting with fertilization and proceeding throughout the entire ontogenetic process. Zebrafish is amenable to such embryonal analysis as well as studies during adulthood. In addition, the zebrafish genome contains a wide range of genes encoding proteins similar to those that form the chaperoning system in humans. Due to the very complex roles played by Hsp60 in cell and tissue homeostasis, the gene is highly conserved during evolution. Nucleotide and amino acid sequences of Hsp60 in zebrafish have 88% of identity with its human orthologous.

- The first aim of my research was the establishment of a zebrafish model as an innovative approach for the study of the molecular basis of SPG13 and define the role of missense mutations V98I.

In the last 18 months of my Ph.D. project, I was at the BIND Department of the University of Palermo and I had the possibility to study a new mutation that occurred in subunit number 5 of CCT complex. This mutation was found in a pediatric patient who is now being treated by the Department Of Sciences For The Promotion Of Health And Childhood "G. D'Alessandro" at the University of Palermo. Thus, I focused my attention on this novel variant, and the main aims were:

- Understanding, with the help of bioinformatics software, the type of mutation and if it causes some alteration of chaperonin molecular anatomy.

- the second objective was to define the morphological changes caused by the mutation in skeletal muscle tissue.

Materials and Methods

1. *In vivo* experiments

1. 2 Study and alignment of human and zebrafish HSPD1/Hsp60 sequences

To evaluate the possibility to perform the genome editing in zebrafish model, I aligned human *VS* zebrafish nucleotides and aminoacids sequences of HSPD1 gene and the corresponding Hsp60 protein, using the program Basic Local Alignment Search Tool (BLAST for proteins and nucleotides) (Figure 5 & 6).

Figure 5

Nucleotides sequences alignment of human and zebrafish (Danio) HSPD1 gene

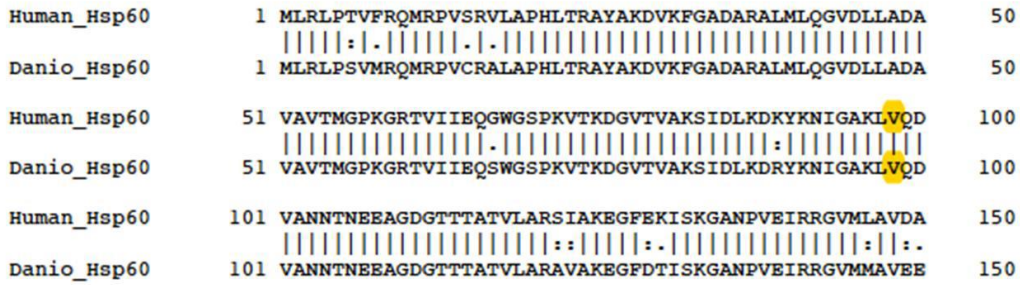

Figure 6

Aminoacidic sequences alignment of human and zebrafish (Danio) Hsp60 protein

Due to the very complex roles played by Hsp60 in cell and tissue homeostasis, this gene is highly conserved during evolution, presenting 88% identity both into the nucleotide and aminoacid sequence between the zebrafish and its human orthologous. The triplet encoding for the Valine in 98 position of the sequence is conserved (yellow underlined nucleotides, and yellow underlined aminoacids respectively in Figure 5 and 6).

1.3 Zebrafish: breeding and reproduction

The fish, inside an aquarium cabinet (Figure 7), are housed in freshwater tanks with a capacity of 3-5 liters each, at a constant temperature of 28 ° C; they are fed three times a day, in the morning with hatched Artemia and the other two with granular food and are subjected to an artificial cycle of 14 hours of light and 10 hours of darkness. Males and females are raised in separate tanks until mating time.

To allow reproduction 1 male and 1 female are joined in 1 liter tanks, equipped with a net in order to prevent the cannibalism of the adults towards the fertilized eggs that are deposited on the bottom. The eggs are laid and fertilized when the light is turned on, after the dark period; they are collected, transferred to Petri dishes containing Fish Water with the addition of 2 parts per million methylene blue and placed to grow in an incubator at 28 ° C, up to the desired stage of development.

Figure 7

Cabinet-aquarium for breeding and reproduction of fish

Water composition for breeding tanks: 34 g Instant Ocean Sea Salt in a liter of deionized water.

Water Fish: 50 ml of water for breeding tanks in 10 liters of deionized water. I used BRASS and TLF (Tuebingen long fin, Tup, Tübingen long fin) zebrafish lines.

Courtesy of Prof. Darius Balciunas (Temple University) I performed CRISPR-Cas9 technique on zebrafish following his protocol[94].

1.3.1 Cas9 mRNA expression plasmid and Cas9 protein

In vitro transcribed zebrafish-optimized nCas9n RNA (Wenbiao Chen lab, http://www.ncbi.nlm.nih.gov/pubmed/23918387 http://www.addgene.org/46757/) is purified using Qiagen MiniElute, diluted to 250 ng/uL and stored at -80°C[94].

1.3.2 HSPD1 gene target

To generate the gRNA that targets the genomic locus, was designed a gRNA cloning vector that harbour the combined features of the crRNA:trascRNA backbone, immediately preceded by a 20-bp “target sequence” (which can be easily added from short annealed oligonucleotides). In this system, a potential genomic target is a stretch of 23-bp genomic sequence that starts from the T7 promoter and ends with the protospacer-adjacent motif (PAM) sequence, NGG, for efficient Cas9 binding.

The following procedures for synthesis of sgRNA were performed according to Prof. Balciunas protocol [94].

1.3.3 sgRNA and ssODN oligonucleotide

Synthesis of sgRNA was carried out following the steps described:

1. PCR was performed using a forward primer (short guide) and a reverse M13F primer harbouring both:

- sequences for T7 promoter
- target gene HSPD1 sequence
- the homology sequence to the sgRNA component of DR274 plasmid (Keith Joung lab, http://www.addgene.org/42250/)

2. Bands from gel were purified with Fermentas gel extraction kit.

3. Second PCR was performed with primers: sgT7- Forward and sgRNA-Reverse. I used a 1 ul of product belonging from previous PCR gel - purified, as template.

4. The template was used for MegaShortscript T7 (Promega) RNA synthesis reaction. The reaction was incubated for 2 hrs.

5. 0.5 uL DNAse, was added and incubated 15 mins

6. 1ul of RNA synthesis 5X diluted was added to 3 ul of RNA loading dye (Fermentas) and visualized on an agarose gel along with RiboRuller RNA ladder and a lane with 5 ul PCR fragments.

7. RNA concentration was estimated based on the gel. RNA was aliquoted for about 60 ng/ul of sgRNA.

Mutating oligonucleotide (ssODN, or oligonucleotide repair) was synthesized and purified by Sigma-Aldrich at 25 nmol synthesis scale followed by desalting. The cells will use oligonucleotide repair as a template during a homology-directed repair (HDR) by inserting the G>A missense mutation for the V98I mutated form within the genome. Actually, taking advantage of the presence of a restriction site for Fok1 (underlined sequence AGGATG in Table 4, G>A substitution in red uppercase was planned within restriction sequence) right close to the site of the G>A missense mutation (triplet green highlighted in Table 4) I design an oligonucleotide repair with a double missense mutation to ensure that the restriction site is lost after HDR (Table 4). This strategy can be used during fish screening of wild type / heterozygous / mutant embryos.

1.3.4 Microinjection in zebrafish embryos

BRASS embryos were injected with a mix of sgRNA and nCas9n RNA. Mutagenesis oligonucleotide was diluted to 50 ng/ul. In total, have been injected 3 ul of mixed RNA and 1 ul of oligonucleotide repair into yolks of embryos.

The freshly fertilized eggs are taken from the tanks and transferred into fish water. The embryos are injected at the stage of 1-2 cells. About 40 embryos are arranged neatly on the side of a glass slide placed in a Petri dish. A total of 150 embryos were injected.

sgRNA-HSPD1-5'CRISPR: 5'-
CGCTAGCTAATACGACTCACTATAGGtatcggagccaagctggttcGTTTTAGAGCTAG
AAATA-3'

HSPD1 WT: 5'-
acaggtataagaatatcggagccaagctgGttcaGgatgtggccaacaacactaatgag
ga-3'

HSPD1 V98I Repair Oligo:5'-acaggtataagaatatcggagccaagctgAttcaAgatgtggccaacaacactaatgaggga-3'

Table 4

CRISPR-Cas9 components

The microinjection is carried out using a micromanipulator (Micromanipulator 5171, Eppendorf) and a microinjector (FemtoJet, Eppendorf; Figure 8).

Figure 8

Microinjection device

1.3.5 Post-injection

At 1-3 dpf, 20 embryos per each mating were frozen and assessed for DNA analysis evaluating the introduced RFLP (FokI restriction sequence), by PCR for HSP60 or with Surveyor assay as indicated by manufacture product (Surveyor® Mutation Detection Kit - S100, IDT).

The embryos, after injection, are grown in an incubator at 28°C always in Water Fish and observed up to the stage of interest. To allow a better observation, the injected embryos are anesthetized with 1X tricaine (Ethyl 3-aminobenzoate methanesulfonate salt, SIGMA; stock tricaina 25X 0.08 g in 20 ml of distilled H2O) in Water Fish and PTU 1X.

Remaining embryos were raised to adulthood, and screened by incross/outcross.

The general procedure was:

- Cross the fish

A cross fish pipeline and procedures associated is reported in Figure 9. F0 larvae could be mosaic for the mutation so, some larvae of each mating must be analysed to characterize a germline transmission. The following mating should be conducted to obtain heterozygous and homozygous stable line. Human V98I mutation occurs in homozygous.

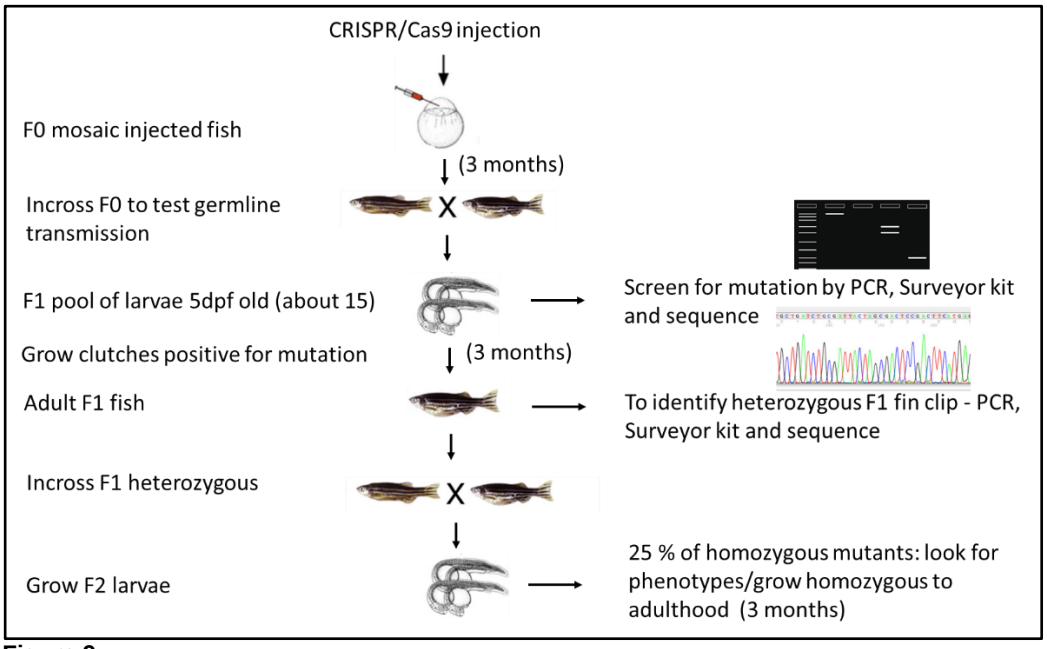

Figure 9

Adapted from Lawson and Wolfe, 2011[95]. Cross fish pipeline and procedures associated

- Freeze a group of 20 embryos for genotyping and keep the rest
- Freeze also individual embryos
- Raise the rest offspring to adulthood
- Analysis/genotyping by fin clips and collecting embryos

1.3.6 DNA extraction from embryos or tails

Frozen live embryos or clipped tail were washed with cleaned water and placed in Eppendorf tubes. According the number of isolated embryos lysis buffer was added to embryos, then I followed the protocol below:

- Pestles embryos or tails
- Add 100 ul DNA extraction buffer and destroy embryos
- Add 5 ul of Proteinase K (2o mg/ml) and mix inverting tubes
- Incubate at 65° for 15 minutes and mix by vortexing every 5 minutes
- Add 7,5 ul potassium acetate 8M and mix by inverting tubes 3-4 times
- Incubate on ice for 15 minutes and mix by vortexing and centrifuge for 25 minutes at 14000 rpm at 4°C
- Carefully transfer the supernatant (100 ul) in new clean tubes
- Add 65 ul of cold isopropanol
- Incubate on ice for 30 minutes and add 1,5 ul glycogen
- Centrifuge for 10 minutes at 14000 rpm at 4°C
- Remove supernatant and add 200 ul of 70% cold ethanol to the pellet
- Incubate 5 minute at room temperature and centrifuge for 5 minute at 14000 rpm at 4°C
- Remove supernatant and all traces of ethanol
- Incubate samples at 50°C with lids opened for 10 minutes

Genomic DNA was resuspended in 30 ul of nuclease free water, incubated ad 50°C for 5 minutes and the DNA concentration was determined with Nanodrop.

1.3.7 PCR to amplify mutated sequence

Nested PCR was performed to amplify mutated sequence. Plasmids are made by a PCR-based approach in which two oligonucleotides carry the appropriate mismatch mutations (Site direct mutagenesis) (Table 5).

Primer	Forward	Reverse
Zebra-HSPD1-ext.	5′-GCCAGTCAAACAAAACCACC	5′-GCCATGAAAATAGCCTTGGT

	ATCC – 3′	TGCTG – 3′
Zebra-HSPD1-int.	5′-GTCATCATTGAGCAGAGCTGGGG – 3′	5′-ACGACTCCAGAGGAAATCGCTCA – 3′

Table 5

Primes for amplification of HSPD1 V98I mutated zebrafish

PCR parameters for 30 cycles:

- 94° for 30 seconds
- 65° for 30 seconds
- 72° for 30 seconds
- 72° for 5 minutes
- 4° hold

1.3.8 DNA electrophoresis in agarose gel

To evaluate the PCR efficiency, PCR product was made to run in an agarose gel. The agarose was dissolved in a 1X TAE buffer in a microwave oven. The concentration of agarose used is 1%. Ethidium bromide was added to dissolved agarose at final concentration of 0.5 g / ml. Finally, gel was poured into an horizontal electrophoresis tray. BioRad mini gel devices are used.

The DNA samples are loaded into the gel after addition of the tracer (10X tracer: 0.4% Bromophenol Blue; 0.4% Xylene Cianol; 50% Glycerol) and then subjected to TAE 1X electrophoresis (40 mM Tris-Acetate; 1 mM EDTA pH 8.0) by applying a ddp of 100 V.

The DNA, after the electrophoretic run, is visualized by means of a UV ray transilluminator and, possibly, photographed.

Bands were cut from gel and purified through QIAquick Gel Extraction Kit.[95]

1.3.9 Sequencing of DNA product

Sequencing of DNA products from PCRs were carried out by GENEWIZ Inc.

2. Bioinformatic analysis

The structural properties of the CCT5 subunit, wildtype and mutated, was obtained starting from the structure of crystallized protein deposited in the Protein Data Bank with accession codes 5UYZ [78].

2.1 Simulation methodology

The structure of the mutant subunit was obtained by changing amino acid residue 224 Leucine with a Valine, using the package Maestro Schrödinger LLC, New York, NY, 2018, version 11.6.010]. MD simulations were performed for 150 ns (in some cases were extended to 200ns), using the GROMACS 5.1.1 package[96,97]. Interactions were described using an all-atoms CHARMM27 force field[98,99]. The simulations for the various systems were performed using a cubic box of NaCl 150mM in explicit TIP3P water solution. Periodic boundary conditions were applied. The force field parameter files and initial configuration for the protein were created by GROMACS utilities programs. The equilibration procedure was performed in several steps, starting from an NVT simulation at 300 K with the protein heavy atom positions restrained to equilibrate the solvent around it, followed by a NPT run at 300 K and pressure at 1 bar, for a 10 ns run. After the equilibration phase, the system was run for a total of 150 ns (200ns) for an NVT production run; the trajectory was saved at a frequency of 10 ps to evaluate dynamical and structural properties. The simulations were always checked versus the root mean square displacement (RMSD) and the energy profile. During the production runs a velocity rescaling thermostat[100] was used for the temperature coupling, with a time coupling constant of 0.1 ps. A Parrinello–Rahman barostat[101] was used for the pressure coupling, with relaxation constant of 1 ps. The equations of motion were integrated through the Leap-Frog algorithm, using a 2 fs time step. The values of cut-offs of the Lennard-Jones and

real space part of the Coulombic interactions were set to 10 Å. The Particle Mesh Ewald (PME) summation method[102,103] was used to evaluate the electrostatic interactions, with an interpolation order of 4 and 0.16nm of FFT grid spacing. The structures shown have been selected by a clustering analysis[104–106] performed by the g_cluster tool implemented in GROMACS package, following the method outlined in an cited article[107]. Selected images and protein manipulation were done using Maestro [Maestro, Schrödinger, LLC, New York, NY, 2018, version 11.6.010] and VMD[108]. All the simulations have been carried out on a workstation equipped with Intel core I7 processor, 32 GB DDR3 system memory and Nvidia GeForce GTX 1080 TI GPU with 11GB DDR5 memory.

3. *Ex vivo* experiments

A skeletal muscle biopsy from the patient's lateral gastrocnemius was obtained following the consent of the parents and the ethics committee. The biopsy was sectioned and processed according to the different research purposes that will be discussed below.

A skeletal muscle from the lower limb of an under 30-year-old volunteer present in our archive was used as a control for this study.

3.1 Histopathology

Skeletal muscle tissue from the patient was excised and fixed in 10% buffered formalin, and embedded in paraffin. Thin sections, obtained from paraffin blocks, were stained with hematoxylin–eosin for histological evaluation and Alcian Blue Pas stain was performed for a better evaluation of ring fibers. Slides were examined, and images captured under bright field with a Leica DM5000 upright microscope (Leica Microsystems, Heidelberg, Germany). Liver sections were examined by an expert pathologist.

3.2 Determination of DNA damage: TUNEL assay

The presence of apoptotic cells, was detected through the study of DNA fragmentation using TUNEL assay, that preferentially labels DNA

strand breaks, generated during apoptosis. The Fluorescein In situ cell death detection kit (Roche Applied Science, Indianapolis, IN) was used.
Sections from mutated biopsy and control skeletal muscle were deparaffinized as described previously and processed for TUNEL analysis. The sections were rehydrated accordingly with PBS and incubated with proteinase K, to avoid false-positive results, at 24°C for 30 minutes, then at 24°C for 8 minutes with a permeabilization solution (0.1% Triton X-100, 0.1% sodium citrate). Indeed, the slides were incubated in the Tunel reaction mixture, including Label solution and enzyme solution, in humidified atmosphere for 60 minutes at 37°C in the dark. Positive controls, using DNase I recombinant (20 U/ml) and negative controls (without terminal transferase) were included in each experiment. Therefore the sections were mounted using the Vectashield Antifade mounting medium (Vector) and examined under CSLM (Confocal Laser Scanning Microscopy), Leica Confocal Microscopy (TCS SP8, Leica Microsystems, Milan, Italy). TUNEL-positive cells were enumerated by counting the labelled cells in eight randomly selected microscopic fields obtained from each specimen at 40× magnification.

3.3 Immunofluorescence

Deparaffinized sections were incubated in the “antigen unmasking solution” (10 mM tri-sodium citrate, 0.05% Tween-20) for 10 min at 75 °C, and treated with a blocking solution (3% BSA in PBS) for 30 min. Next, the primary antibody (anti- α-actin, rabbit polyclonal, Sigma A2066; anti-laminin, mouse polyclonal AB2034, Millipore; anti-CCT5, rabbit polyclonal, TA308298 Origene; anti-Pax7 mouse monoclonal, AB_528428, Hybridoma Bank) diluted 1:50, was applied, and the sections were incubated in a humidified chamber overnight at 4 °C. Then, the sections were incubated for 1 h at 23 °C with a conjugated secondary antibody (anti-rabbit IgG–FITC antibody produced in goat, F0382, Sigma-Aldrich; anti-mouse IgG-TRITC antibody produced in goat, T5393, Sigma-Aldrich). Nuclei were stained with Hoescht Stain Solution (1:1,000, Hoechst 33258, Sigma-Aldrich) (Table 6). The slides were treated with Perma Fluor

Mountant (Thermo Fisher Scientific, Inc. Waltham, MA, USA) and cover slipped. The images were captured using a Leica Confocal Microscope TCS SP8 (Leica Microsystems).

Method	Antigen	Type and source	Supplier	Catalogue Number	Dilution
IF	CCT5	Rabbit polyclonal	Origene	TA308298	1:50
IF	laminin	Mouse polyclonal	Millipore	AB2034,	1:50
IF	α-actin	Rabbit polyclonal	Sigma A2066	A2066	1:50
IF	Pax7	Mouse monoclonal	Hybridoma Bank	AB_528428	1:50

Table 6

Primary antibodies used for immunofluorescent and double immunofluorescence (IF).

3.4 Double immunofluorescence (IF)

To assess the presence of Pax7 positive fibers, and to evaluate them in the laminin context, a double immunofluorescence was carried out.

The immunofluorescence was performed as previously described by Marino Gammazza and colleagues [109]. Briefly, sildes of mutated muscle tissue and healthy control were deparaffinized and incubated in the “antigen unmasking solution” (10 mM tri-sodium citrate, 0.05% Tween-20) for 10 min at 75 °C, and treated with a blocking solution (3% BSA in PBS) for 30 min. After that the sections were incubated with the first primary antibodies Pax-7 diluted 1:50, overnight at 4°C. The day after, the sections were incubated with the second primary antibody anti-laminin, diluted 1:50, overnight in a humidified chamber at 4°C. Once again, slides were incubated with fluorescent secondary mouse IgG antibody TRITC conjugated (from Sigma-Aldrich), diluted 1:250, for 1h at RT. Therefore, we used FITC conjugated rabbit IgG secondary antibody (from Sigma-Aldrich), diluted 1:250, for 1h at RT in a moist chamber. The nuclei were counterstained with Hoechst 33342 (Sigma-Aldrich) for 15 minutes at RT.

Finally, the slides were covered with drops of PBS and mounted with coverslips, using a drop of Vectashield (Vector, Burlingame, CA). Imaging was immediately performed with an upright fluorescent microscope Leica DM5000. The fibers positivity of both markers (“Merge”) was assessed through the ImageJ Free software (NIH).

3.6 Total RNA Extraction and Retro Transcription PCR.

RNA from both mutated and healthy skeletal muscle tissue , was obtained, as previously described by Rappa and colleagues [110], by the use of TRI Reagent© (Catalog Number T9424, Sigma-Aldrich, Saint Lois, MO), which is a mixture of guanidine thiocyanate and phenol that allow to isolate simultaneously RNA, DNA, and protein.

Frozen at - 80°C pieces of biopsies were defrosted on ice and each sample was homogenized in 1 ml of TRI Reagent© and subsequently centrifuged at 12000 x g for 10 minutes at 4°C to remove the insoluble material. Then, 0.2 ml of chloroform was added to the samples. After 15 minutes, the mixtures were centrifuged at 12000 x g for 15 minutes at 4°C, to separate the RNA phase from proteins and DNA, and RNA phase was transferred to a fresh tube and then 0.5 ml of isopropanol was added. After 10 minutes, the samples were centrifuged at 12000 x g for 10 minutes at 4°C. The supernatant was removed and the RNA pellet was added to 1 ml of 75% ethanol and then shaken. The mixture was centrifuged at 7500 x g for 5 minutes at 4°C. Finally, we dissolute the air-dried RNA in 50µl of RNase/DNase-free H_2O by repeated pipetting with a micropipette at 55–60 °C for 10–15 minutes.

The concentration of the RNA extract was determined using Thermo Scientific NanoDrop ND-2000 1-position Spectrophotometer (Thermo Scientific Massachusetts, USA).

cDNA was synthesized, as described by Campanella and colleagues [111], using ImProm–II Reverse Transcriptase (Catalog Number A3800, Promega Corporation, Madison, WI, USA). To obtain 200 ng of cDNA, twenty microliters of mixed solution with RNA template, 0.5 µg Oligo(dT) primers, 6mM MgCl2, reaction buffer 5X, 1 µL dNTP (0.5 mM mixture of

dATP, dCTP, dGTP, and dTTP), 20U RNase inhibitor, 1 µL ImProm-II reverse transcriptase, and nuclease-free distilled water was incubated at 25℃ for 5 minutes and then at 42℃ for 90 minutes. To inactivate reverse-transcriptase, the mixture was incubated at 70℃ for 15 minutes. Thereafter, cDNA, was amplified using the GoTaq qPCR Master Mix (Promega Corporation, USA). The reaction mix was prepared with cDNA template, upstream and downstream PCR primers and GoTaq® qPCR Master Mix, 2X. The cycling program was carried out with the Rotor Gene Q, Qiagen (Qiagen, Milan, Italy), using the following steps: Hot-Start Activation, 1 cycle at 95°C for 2 minutes; denaturation, 40 cycles at 95°C for 15 seconds; annealing/extension at 60°C for 60 seconds; dissociation, 1 cycle at 60–95°C. The mRNA levels were normalised to the levels obtained for (GAPDH). Changes in the transcript level were calculated using the 2-ΔΔCt method [112]. The cDNA was amplified using the primers indicated in Table 7.

Primer	Forward	Reverse
Homo CCT5	5'-CAACACCTGGACAAGATCAGCG-3'	5'-TCTCAGCCATCTGTCGGTGACA-3'
Homo GAPDH	5'-TCCCTCCAAAATCAAGTGGG-3'	5'-GGCAGAGATGATGACCCTTT-3'

Table 7

Forward and reverse primers used for the polymerase chain reaction.

Results

1. *In vivo* analysis

1.1 CRISPR/Cas9 evaluation through Surveyor assay of F0

CRISPR systems in eubacteria and archaea is like an “immune system” that use small RNAs and CRISPR-associated proteins (Cas) proteins to target and cleave invading foreign DNAs. The type II CRISPR systems from Streptococcus pyogenes is composed by an endonuclease Cas9 and two small RNAs, CRISPR RNA (crRNA) which in turn anneal to a trans-activating crRNA (tracrRNA). They are sufficient to direct Cas9-mediated cleavage of target DNA. During the years has been used a single guide RNA (gRNA) chimera that mimics the crRNA:tracrRNA complex (Figure 10). The gRNA can guide Cas9 nuclease to introduce site-specific DNA double-stranded breaks in vitro and in mammalian cell lines, bacteria, yeast, zebrafish, and mice[113].

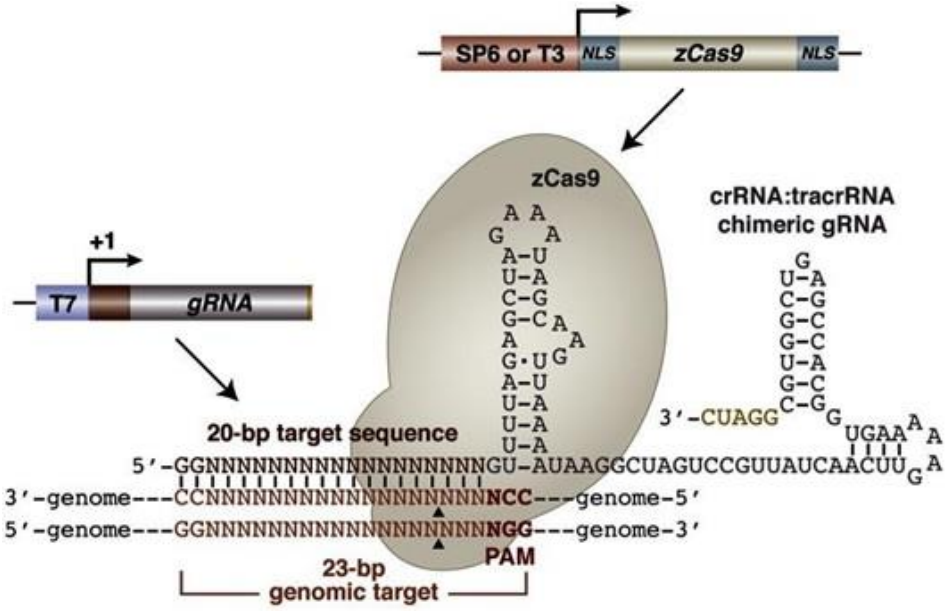

Figure 10

Genome editing in zebrafish using a CRISPR/Cas9 system[113]

I create an sgRNA as described in Material and Methods and 1-cell zebrafish embryos were microinjected with a mix of single RNA guides (sgRNA) and nCas9n RNA.

Firstly, I isolated 3 samples of 5 days post fertilization (dpf) larval stage, each of which will contain 10-15 F0 larvae, which would suggest at least a 20% frequency of integration. After genomic DNA extraction from each batch, these DNAs will be used to amplify, by PCR, a fragment of ~200bp spanning the two CRISPRs sites subsequently analysed by Surveyor assay analysis for the presence of indels mutations.

The Surveyor assay allows quick and easy detection of mutations and polymorphisms in DNA. The Surveyor Nuclease, a member of the CEL family of mismatch-specific nucleases, recognizes and cleaves mismatches due to the presence of single nucleotide polymorphisms (SNPs) or small insertions or deletions.

- Detect base-substitution and insertion/deletion mismatches
- Identify mutations in DNA fragments up to 3.5 kb with a single reaction
- Quickly determine the number of mutations by observing the number of cleavage products

Although this essay cannot confirm the presence of the desired mutation, this allows me to define the quality of the CRISPR / Cas9 technique.

In total about 150 wild type embryos were microinjected. The first day (Figure 11) (1° inj.) were microinjected for CRISPR/Cas9_V98I, 50 embryos coming from the mating of a male and a female of BRASS line. About 100 other embryos were microinjected the following day (2 ° inj.) from the mating of a BRASS couples.

I performed Surveyor assay of F0 embryos and run a 2% agarose gel with 3 sample of the 1°inj. and 4 samples of 2° inj. I run the gel positioning for each sample the DNA undigested (U) and the DNA digested (D). I used a 100 base pairs marker of molecular weights at either end of the gel.

In particular, two samples showed the presence of a double band (indicated by the arrows).

Figure 11

Surveyor assay from F0

1.2 Sequencing of positive samples of F0

To evaluate the indels mutation the two samples were sent for sequencing, and as shown in Figure 12, a certain mismatch of the sequence right near the PAM sequence (sequence red in Figure 9) was detected where I expected to find the missense mutation of interest.

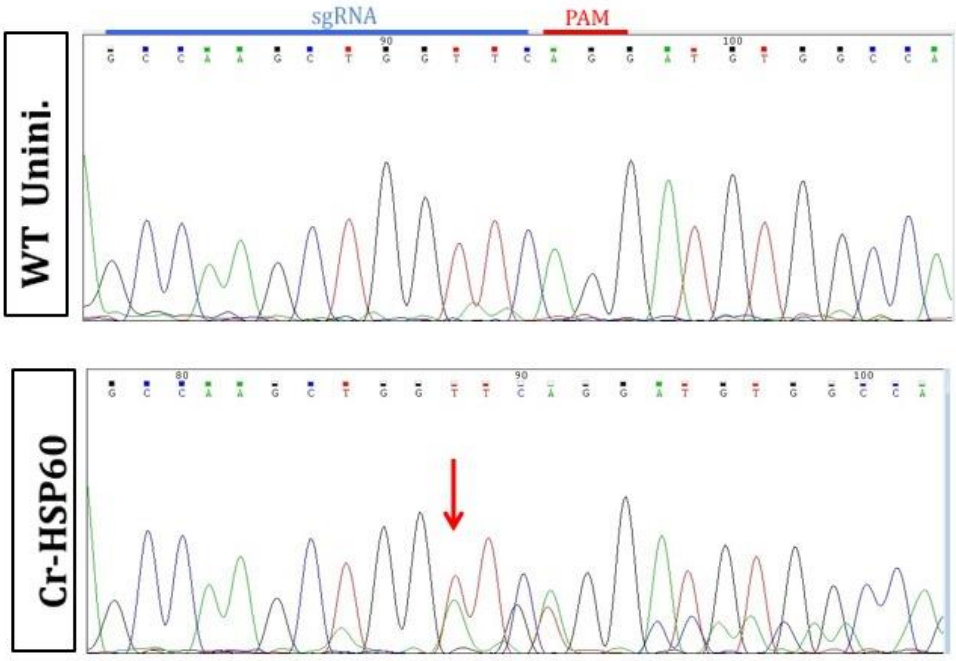

Figure 12

Sequencing of positive samples of F0

1.3 Surveyor assay from F1 generation

Since fish becoming from F0 generation are mosaic for mutation, to evaluate germline transmission F0 fish male and female were mated in incross (F0xF0) and outrcross (F0xTLF wild type not injected fish) manner to get F1 generation. F1 pool of larvae (about 15 5dpf as I did for F0 generation) of each mating were collected and, DNA extraction, PCR for HSPD1 gene and Surveyor assay to detect mismatches were performed. Gel at 2% agarose run with product of surveyor assay with the same modality before described: an undigested and a digested sample becoming from the same batch (Figure 13, 14 and 15).

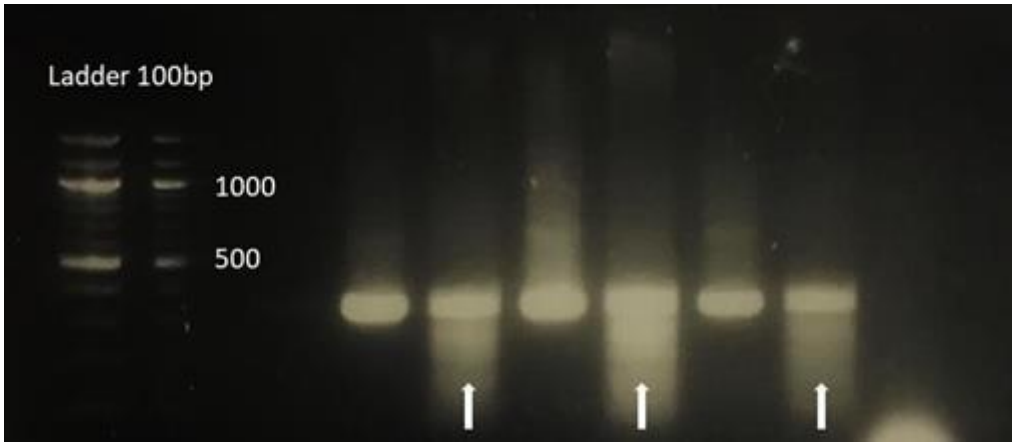

Figure 13

Surveyor assay F1 (#1Male x Female TLF wt outcross). Undigested and digested surveyor product in triplicate

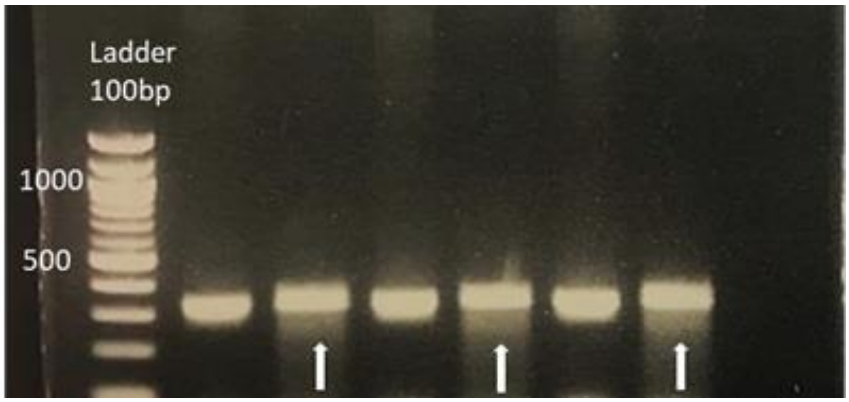

Figure 14

Surveyor assay F1 (**#2Male** x Female TLF wt outcross). Undigested and digested surveyor product in triplicate

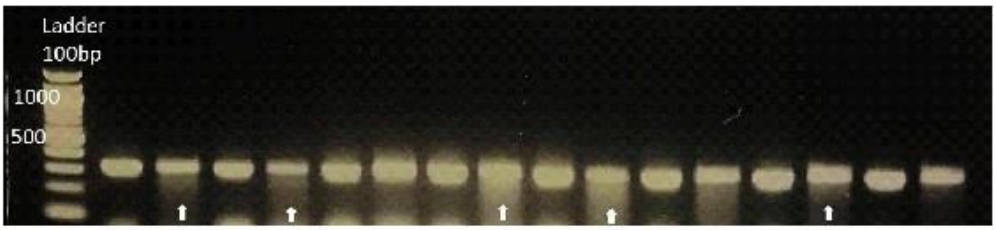

Figure 15

Surveyor assay F1 **(#3_#4_#5Male** x Female TLF wt outcross). Undigested and digested surveyor product in triplicate and the last one in duplicate.

Only 5 males (male #1 in Figure 13, male #2 in Figure 14, and male #3, #4, #5 in Figure 15,) mated with non-injected wild type TLF females were

selected because the gel for the surveyor assay showed, albeit slightly, a double band index of the mismatch.

The 5 selected fishes were newly mated and the same analysis were performed but it was not possible to reconfirm the data.

2. Bioinformatic analysis

2.1 The patient mutation causes the disease

The patient is a young girl of 8 y.o. positive for the c.670C>G mutation that determine the aminoacidic substitution of a leucine with a valine in position 224 (L224V) on the protein/subunit 5 (CCT5) of the CCT chaperonin. Main symptoms and clinical features are epileptiform encephalopathy, microcephaly, severe psychomotor retardation and severe hypotonia.

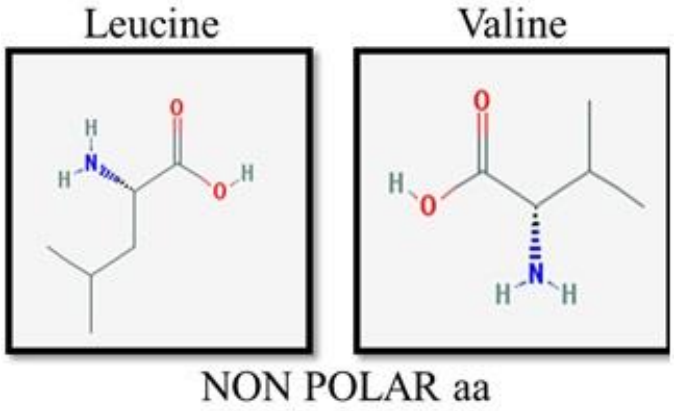

Figure 16

Amino acids involved in point mutation

The substitution of Leucine with Valine from the aminoacid point of view had raised some doubts if it was the actual cause of the pathology, since it is a substitution of a non-polar amino acid with another non-polar amino acid. Despite L224V and H147R[50] mutation before reported occur on the same subunit (CCT5), the course of the diseases does not seem to be the same. The first investigations started with bioinformatics studies using disease prediction software:

1. PlyPhen-2 report
2. Mutation t@sting

3. PROVEAN

The response of the software was:

- ❖ Prediction disease causing
- ❖ PROBABLY DAMAGING with a score of 1.000 (maximum)
- ❖ Deleterious

2.2 Analysis of L224V mutation

As reported in literature[114] CCT5 subunit has a specific function within the complex CCT. It has the function of strongly hydrolyse ATP, working together with other neighbouring subunits as a motor for the whole complex.

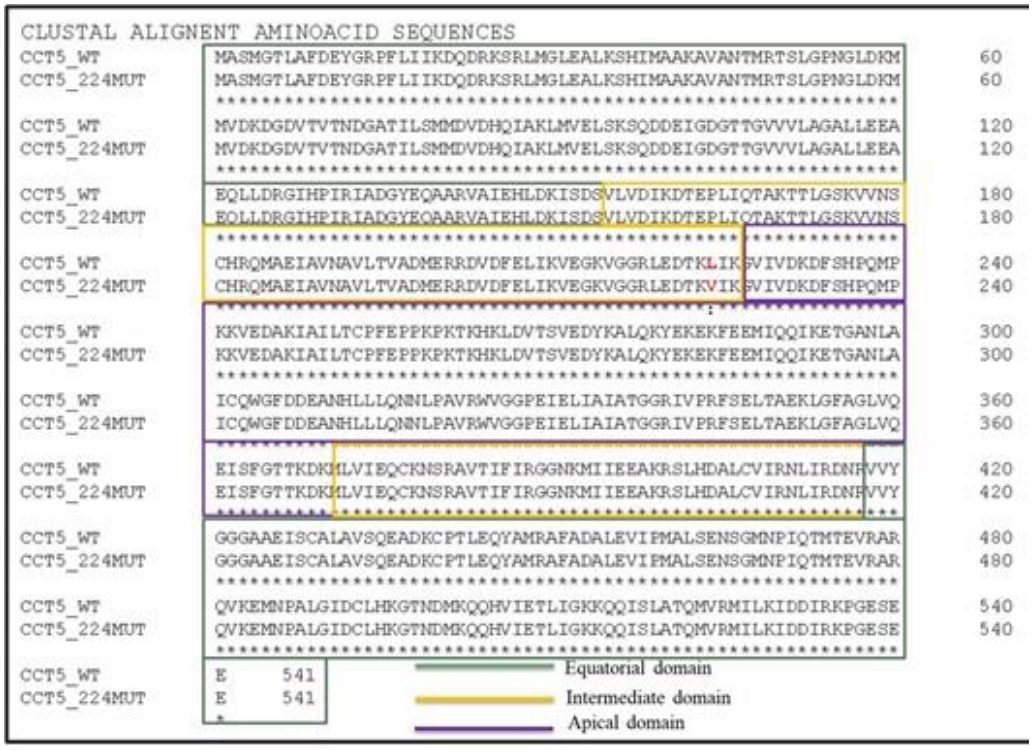

Figure 17

Clustal alignment of CCt5 wildtype and mutated sequence. Insert in different coloured box are shown the sequence segments of equatorial (green), intermediate (yellow) and apical (violet) domains

Study and alignment of CCT5 wild type and mutate forms was conducted using Clustal Omega multiple sequence alignment program. As shown in Figure 17 is possible define that L224V mutation occurs in the

intermediate domain of subunit, and not at the equatorial domain which has the hydrolysing ability (as for H147R mutation). It should be borne in mind that the linear amino acid sequence of the CCT5 subunit (Figure 17) shows that the domains are not sequentially encoded but there are two amino acid strings for the equatorial domain (from 1 to 154 amino acid residue (1°); from 418 to 541 amino acid residue (2°)), two for the intermediate domain (from 155 to 226 amino acid residue (1°), string in which occurs the mutation; from 381 to 417 amino acid residue (2°)), and one for the apical domain (from 227 to 378 amino acid residue).

2.3 Simulations of CCT5 subunits, wilde type and mutated (L224V)

How CCT complex acts during its cycle to bind and release a folded protein is not yet fully known. Surely, we know that should be an open conformation of the whole complex to bind nucleotide (ATP) and substrate (e.g. actin or tubulin), following by a close conformation to hydrolyse ATP in ADP and simultaneously fold the substrates, then complex has to release folded proteins and ADP to be start next cycle. During this process several conformational changes of each subunit rule over the functioning of CCT, if a subunit domain is not in its correct conformational state, it cannot make its contribution by invalidating the functionality of the entire complex.

In order to evaluate possible alterations of CCT5 conformational state due to mutations, simulations of CCT5 wildtype and CCT5_L224V mutated subunit without nucleotide, with ATP or ADP were performed.

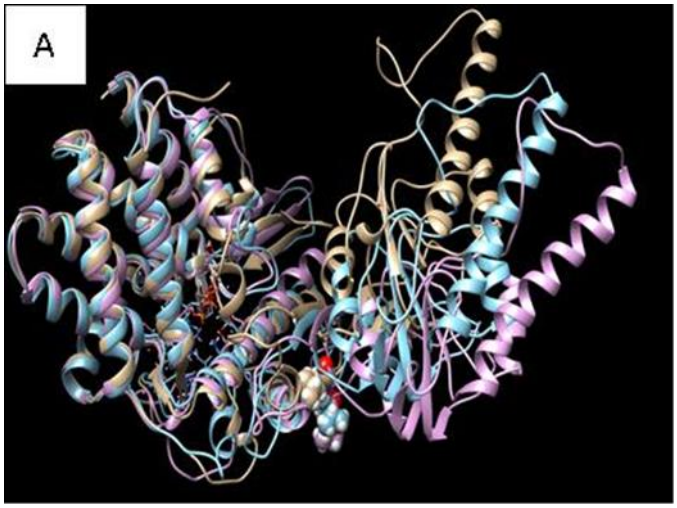

Image A

Superposition of the most probable conformations obtained from the simulation of wild type CCT5 without nucleotide (gold), linked to ATP (lila) and linked to ADP (cyan). The image shows how the protein assumes different conformations in the three states taken in examination, especially at the level of one's apical domain.

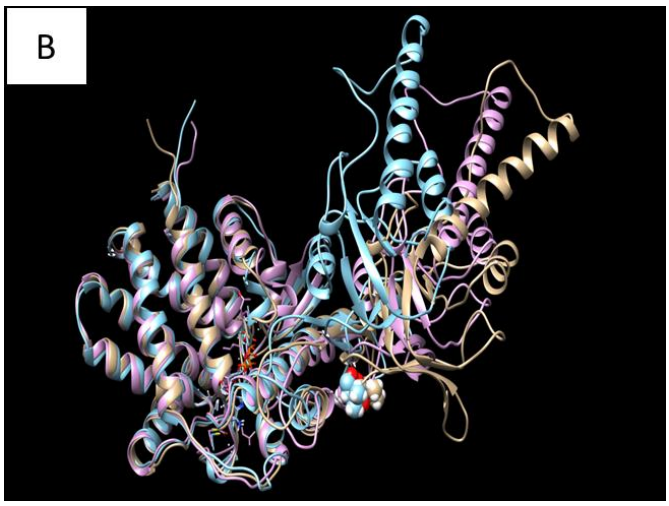

Image B

Superposition of the most probable conformations obtained from the simulation of CCT5 mutated without nucleotide (gold), linked to ATP (lila) and linked to ADP (cyan). The image shows how the protein assumes different conformations in the three states examined, especially at the level of one's apical domain.

The conformations are completely different compared to the equivalent conformations of the wild type protein. In fact, starting from the conformation without any nucleotide, the mutated protein appears more relaxed at the level of its apical domain compared to the wild type protein.

To better understand the alterations, other simulation and superposition illustrated in Table 8 were performed:

	Status of CCT5 subunit	**Nucleotide**	**Colour**
Superposition A	Wilde type	/	Gold
	Wilde type	ADP	Cyan
	Wilde type	ATP	Lila
Superposition B	Mutated_L224V	NO	Gold
	Mutated_L224V	ADP	Cyan
	Mutated_L224V	ATP	Lila
Superposition C	Wilde type	/	Orange
	Mutated_L224V	/	Blue
Superposition D	Wilde type	ATP	Orange
	Mutated_L224V	ATP	Blue
Superposition E	Wilde type	ADP	Orange
	Mutated_L224V	ADP	Blue

Table 8

Superposition of CCT5 wildtype and mutated CCT5 subunit

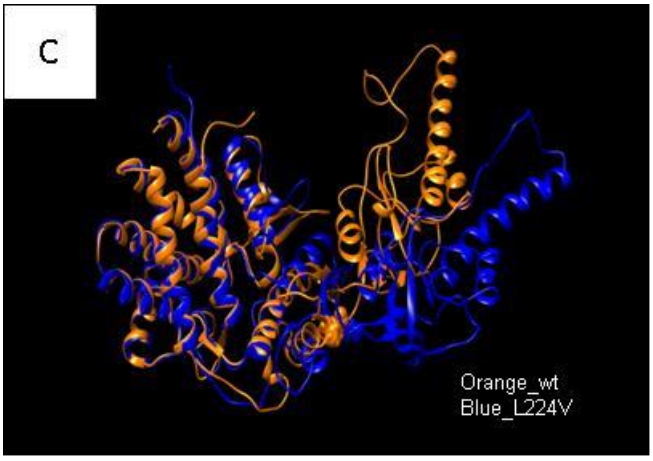

Image C

Examining the superposition between the wild type and the mutated subunit both without nucleotide (**Image C**), it is possible confirm what has been stated before. A greater opening of the mutated protein (in blue), especially at the level of the helix α9, compared to the wild type protein (in orange) in shown.

Image D

In the status linked to ATP CCT5_L224V subunit (lila image B and blue **Image D**), the helix α9 turns out to be more closed as against to the condition without nucleotide (lila image A and blue image C). This conformation is contrary to that observed for the wild type protein, in which the binding of the ATP involves a greater opening of the lid domain (helix α9) (lila image A and orange image D) compared to the condition without nucleotide (gold image A and orange image C).

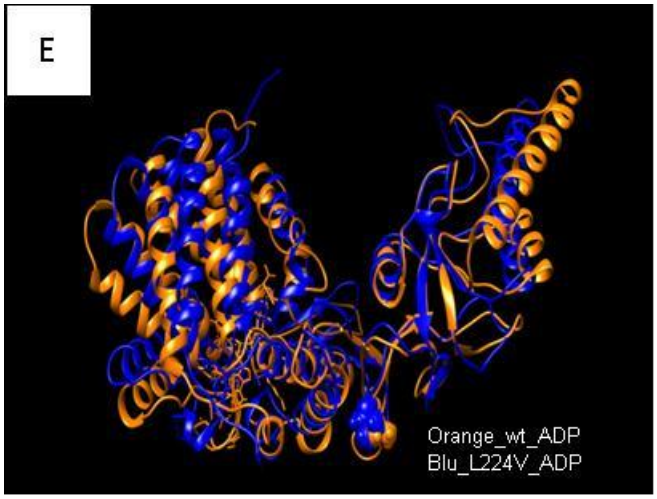

Image E

Finally, the binding of ADP to the mutated protein (cyan B and blue **Image E**) results in greater closure of the lid compared to the other two conditions (protein mutated without nucleotide or with ATP) (gold and lila image B; blue image C and D), unlike the wild type protein (image A).

This situation, however, is closer to what was assumed regarding the folding cycle, since the release of Pi should promote a slight but not complete re-opening in order to release the substrate. However, analysing the image of the overlap of the wild type protein and of the mutated protein both linked to ADP (image E) there are no large differences at the level of the apical domain but nevertheless a certain instability along the whole subunit which in the previous simulations did not occur, was observed.

From the analysis of these simulations we can certainly observe a different conformation of the mutated protein with respect to the wild type protein in all three conditions (without nucleotide, with ATP or ADP).

2.3.1. Analysis of CCT5 simulations: radius of gyration *versus* time

The radius of gyration is a mathematical expression of the distribution of masses within the molecule. Describes how the components of an object are distributed around its rotation axis. The folding process is typically accompanied by a significant decrease in the SASA (Solvent Accessible Surface Area) or alternatively also called “radius of gyration”. The radius of gyration is therefore an indicator of the folding process, determines the protein structure compactness and describes the equilibrium conformation of a total system.

Graph A **Graph B**

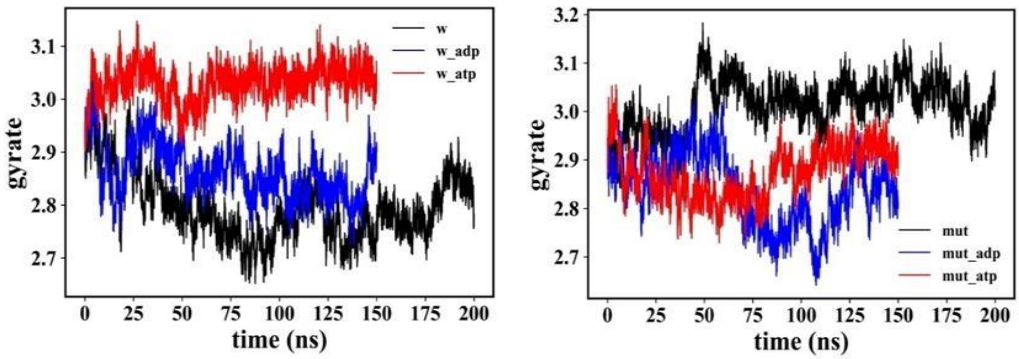

Graph A shows the comparison of the radius of gyration of CCT5 wild type subunit as a function of time, without nucleotide (in black), linked to ATP (in red), and linked to ADP (in blue). The initial values are the same for all three conditions, however within the first 25 ns the trends begin to move away from each other: the radius of gyration of the wild type subunit linked to ATP (in red) increases slightly, then decreases again and finally remains at a constant value and within a given range for the rest of the simulation lasting 150 ns; the radius of gyration of wild type protein bound to ADP (in blue) remains swinging in a wider range and also shows a more fluctuating trend; finally the radius of gyration of the wild type protein without nucleotide (in black) tends to decrease slightly with respect to the starting value within the first 100 ns and subsequently shows a fluctuating trend for the rest of the simulation lasting 200ns.

Graph B shows the comparison of the gyration radius as a function of the time of CCT5 mutated without nucleotide (in black), linked to ATP (in red), and linked to ADP (in blue). Under ATP- and ADP-bound conditions, the radius of gyration of the protein is less than the condition without nucleotide (in black). Also in this case the starting values are the same and remain so within the first 25 ns; the radius of gyration of the mutated protein linked to ATP (in red) remains more constant than the others even though it oscillates in a fairly wide range; the radius of gyration of the mutated protein bound to ADP (in blue) remains around the starting value in the first 60 ns and shows a much more variable trend in the rest of the simulation lasting 150 ns; finally, the radius of gyration of the mutated protein without nucleotide (in black) remains constant within the first 50 ns, to then increase in a sudden manner and again remain constant, even though it swings in a fairly wide range for the rest of the simulation of the duration of 200ns.

Therefore even the radius of gyration analyses show that the two conformations, wild type and mutated CCT5 subunit in the three conditions, do not have the same trend. In particular, the radius of gyration

of the mutated protein without nucleotide has a totally opposite trend compared to its wild type counterpart.

2.3.2 Root Mean Square Displacement (RMSD) CCT5 simulations

Root Mean Square Deviation (rmsd), is a way to indicate the average distance of structurally equivalent atoms. Since from the simulations it is clear a greater mobility of the apical domain compared to the intermediate and equatorial domain, both in the wild type protein and in the mutated one, the RMSD of this domain has been examined in comparison to all others domain, within wild type or mutated subunit in the three different conditions (without nucleotide, with ATP and with ADP).

Moreover, RMSD of the apical domain (which goes from the amonoacidic position 227 to 378) of the wild protein was compared to that of the mutated protein in the three conditions (without nucleotide, with ATP and with ADP).

Graph C

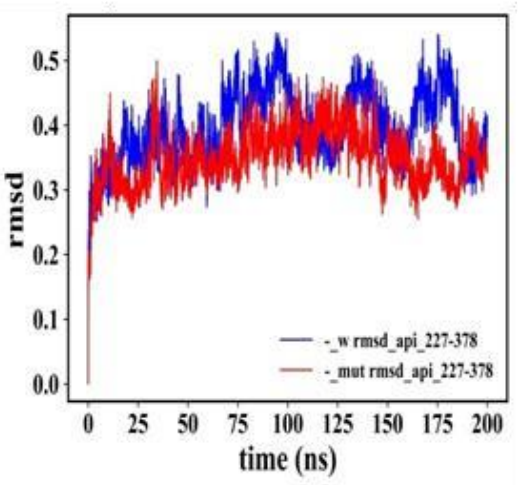

In the condition without nucleotide (**Graph C**) the RMSD of the wild type subunit apical domain (blue) and that of the mutated protein (red) have an overlapping value in several phases of the simulation lasting 200 ns. However the RMSD of the apical domain of the wild type subunit seems to swing in a wider range and seems to have a more fluctuating trend from 100 ns onwards

Graph D

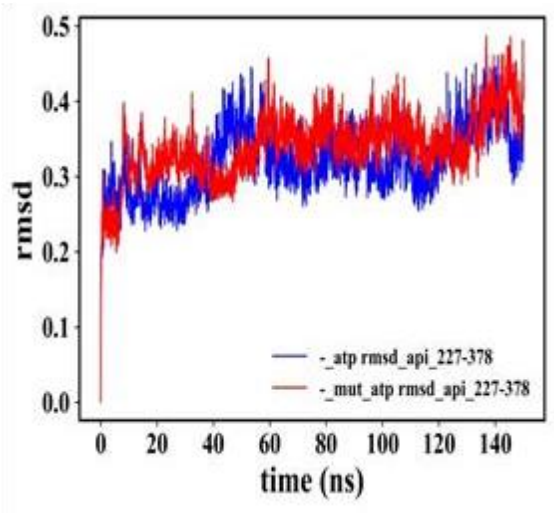

The **Graph D** compares the RMSDs of the apical domains of the wild type and mutated subunit both linked to ATP. RMSDs overlap and have a variable trend during the whole simulation swing in a range of about 0.2 nm.

Graph E

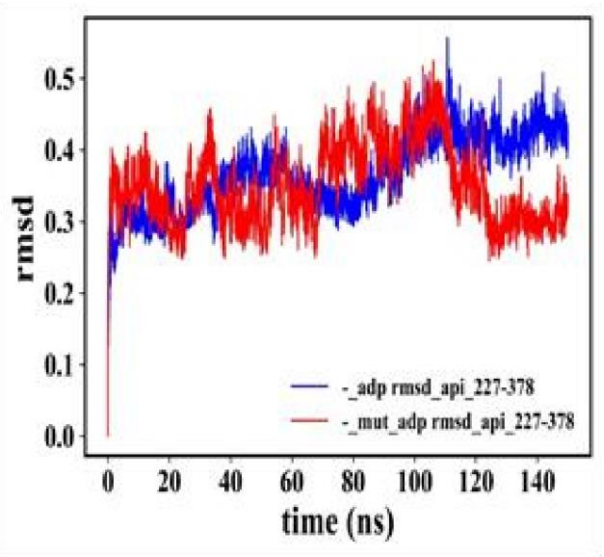

Graph E shows the comparison between the RMSDs of the wild type (blue) and mutated (red) apical domain protein both linked to ADP and again it is observed that the two RMSDs overlap in several parts of the simulation despite having a different trend. In fact, the wild type (in blue)

tends to gradually increase, instead the mutated (in red) has a more variable trend.

To better understand which string coding domain, or part of a domain, is involved in molecular anatomy adjustment of CCT5 subunit, I evaluated the RMSDs of different strings-domains of wild type and mutated proteins. Shifts of RMSDs analysis were assess in apical and first (1°) intermediate domain in all three conditions (without nucleotides, with ATP, with ADP). Graphs are reported below:

Graph F **Graph F1**

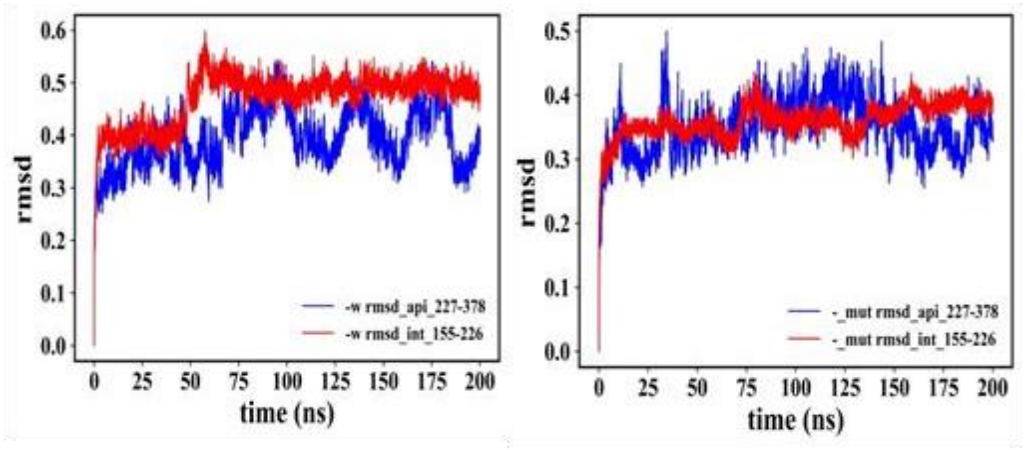

Graph F shows RMSDs of apical wild type domain (blue) with intermediate (1°, red) wild type domain **without nucleotide**. The latter shows a constant trend in the initial phase, then around 50 ns it undergoes a rapid increase and reaches a value which again remains constant until the end of the simulation. Furthermore, in several phases it overlaps, while in others it is larger than the RMSD of the apical domain.

Graph F1 shows the RMSDs of the apical domain (in blue) and the intermediate domain (1°, red) in the mutated protein without nucleotide. The second shows three different phases (0-75ns, 75-125ns and 125-200ns) during which it remains constant. Moreover, it overlaps during the whole simulation to the RMSD of the apical domain.

Graph G **Graph G1**

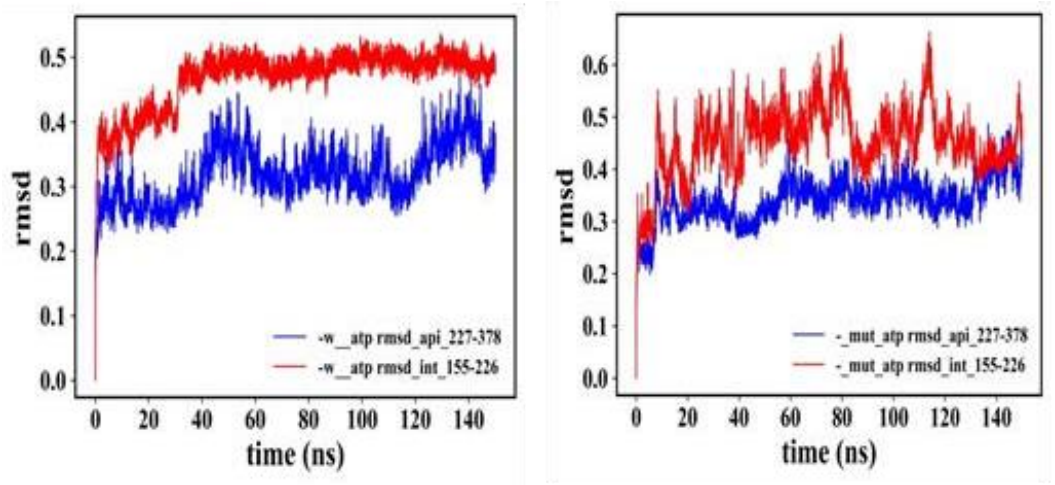

Graph G shows RMSDs of apical wild type domain (blue) with intermediate (1°, red) **wild type** domain **with ATP**. Again, as observed for the wild type protein without nucleotide (graph F), the RMSD of the first intermediate domain undergoes a slight increase after the first 40 ns and then remains constant throughout the simulation and greater than the RMSD of the apical domain.

Graph G1 shows the RMSDs of the apical domain (in blue) and the intermediate domain (1°, red) in the **mutated** protein **with ATP**. For the first time, compared to all the previously analyzed cases, the RMSD of the first intermediate domain is considerably much more variable. The trend is clearly different from that observed for the wild type protein with ATP (Graph G).

Graph H **Graph H1**

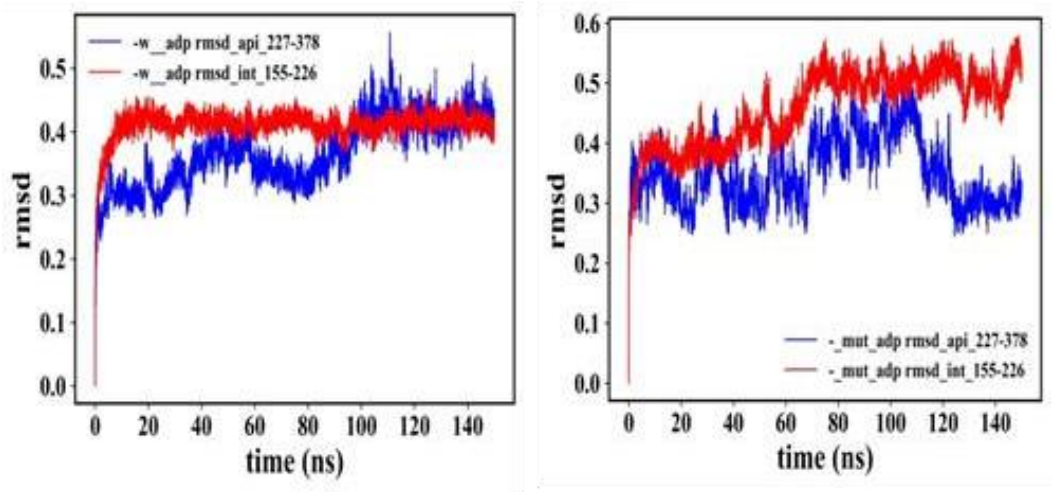

Graph H shows RMSDs of apical wild type domain (blue) with intermediate (1°, red) **wild type** domain **with ADP**. The latter remains constant throughout the simulation and is larger than the RMSD of the apical domain in the first 90 ns and superimposable to it in the rest of the simulation. Furthermore, the RMSD of the first intermediate domain of the protein bound to ADP is slightly lower than those of the first intermediate domain of the protein without nucleotide (graph F) and linked to ATP (graph G).

Graph H1 shows RMSDs of apical wild type domain (blue) with intermediate (1°, red) **mutated** domain **with ADP**. The RMSD of intermediate domain has a variable trend in that it undergoes an increase between 60 and 80 ns and swings in a wide range, overlapping or remaining a little greater than the RMSD of the apical domain which has an even more variable trend. The trend of the RMSD of the intermediate domain is more variable than that observed in the wild type subunit with ADP in which it maintained a more constant value (graph H), like that observed in the mutated protein without nucleotide (graph F1) and much less variable than that observed in the mutated ATP-bound protein, in which the RMSD of the intermediate domain is the one with the most variable trend (graph H1).

While the previous simulations seemed to mark a substantial difference between the conformation of wild type subunits and mutated only in the absence of nucleotide, RMSD analyzes show that the mutated subunit appears to move away from the wild type condition in all three conditions, in particular the first (1st) intermediate domain, where the mutation takes place, is particularly affected by the change. In association with this data, also the RMSDs of the apical domain confirm a consequent instability of the mutated domain in all the analyzed conditions. All the other domains instead show a more or less constant RMSD.

2.3.3 Heat maps of simulations

To know which amino acid caused the anatomical changes of the molecule, and to confirm the observations obtained so far, heat maps were produced. They show the RMSDs of the individual amino acid residues during simulations in Angström unit.

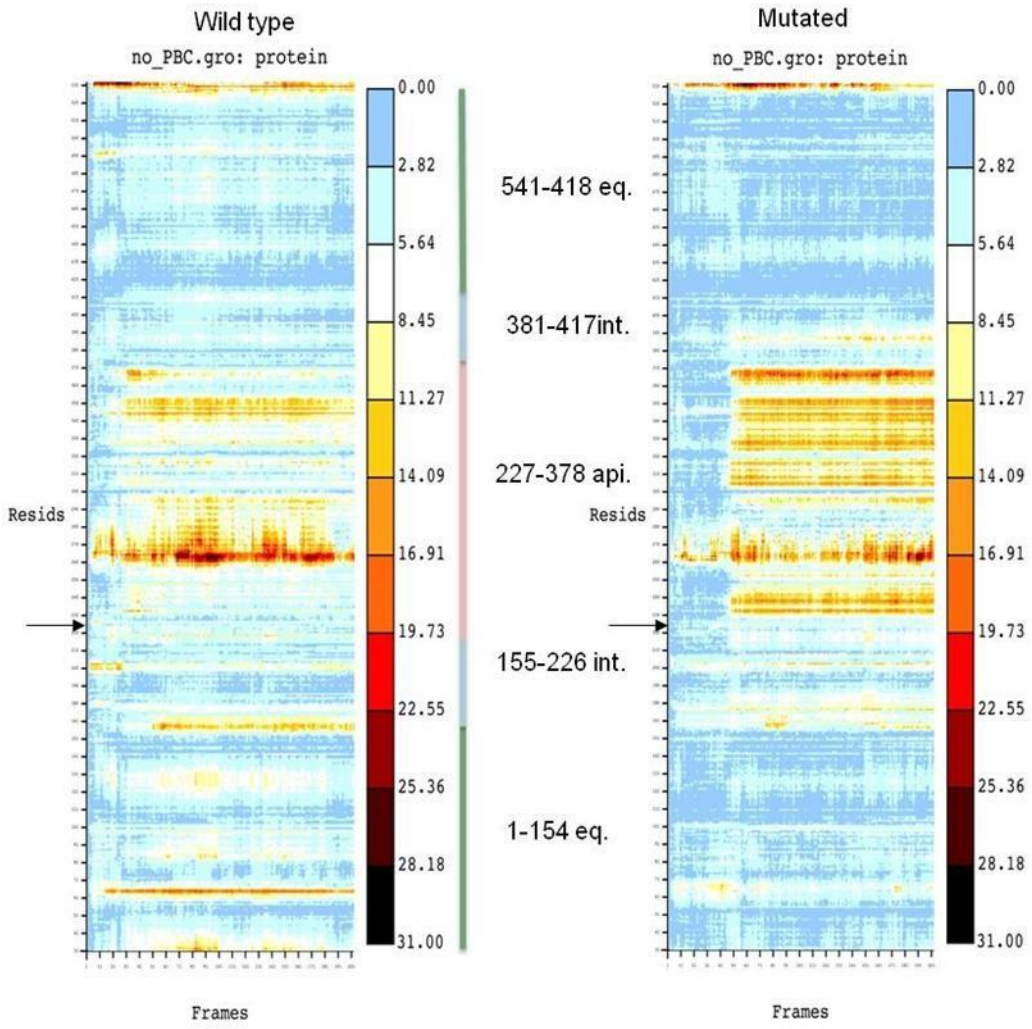

Figure 18

Heat maps of wild type and mutated CCT5 subunit without nucleotide: in wild type map a wider area of heat is observed only in the region between the residues 260-270 and from 230 to 250 residue, both of which corresponds to apical domain. In the mutated subunit the area with a wider heat is observed from 230 to 370 residue, which covers 1) few nucleotides of intermediate domain immediately after the 224 position where the point mutation occurs (indicated by the black arrow), and 2) the entire apical domain.

Since the apical occurs in the recognition of a large range of proteins substrate, it is the domain with more heterogeneity between subunits and it is less conserved during evolution[50].

Helix-10 of apical domain (residues $_{309}$EANHLLLQ$_{316}$) and proximal loop region (residues $_{234}$FSHPQMPK$_{241}$) are involved in substrate-binding. Furthermore, above substrate-binding region, the extended α-helix (helix-9) of apical domain acts as a built-in lid to close the CCT cavity and is

linked to an apical loop ($_{259}$KPKTKHK$_{265}$) which create an highly charged regions probably involved in substrate interaction[50].

The heat maps of the mutated CCT5 subunit describes how, due to the mutation, there is a large instability of the apical domain in the absence of nucleotide as opposed to what is shown by the heat map of the wild type subunit. We could also say that this phenomenon can be observed starting from the 224 position to rise. The remaining part of the subunit (from position 224 to descending) is characterized by a strong and perhaps excessive stability, especially of the equatorial domain.

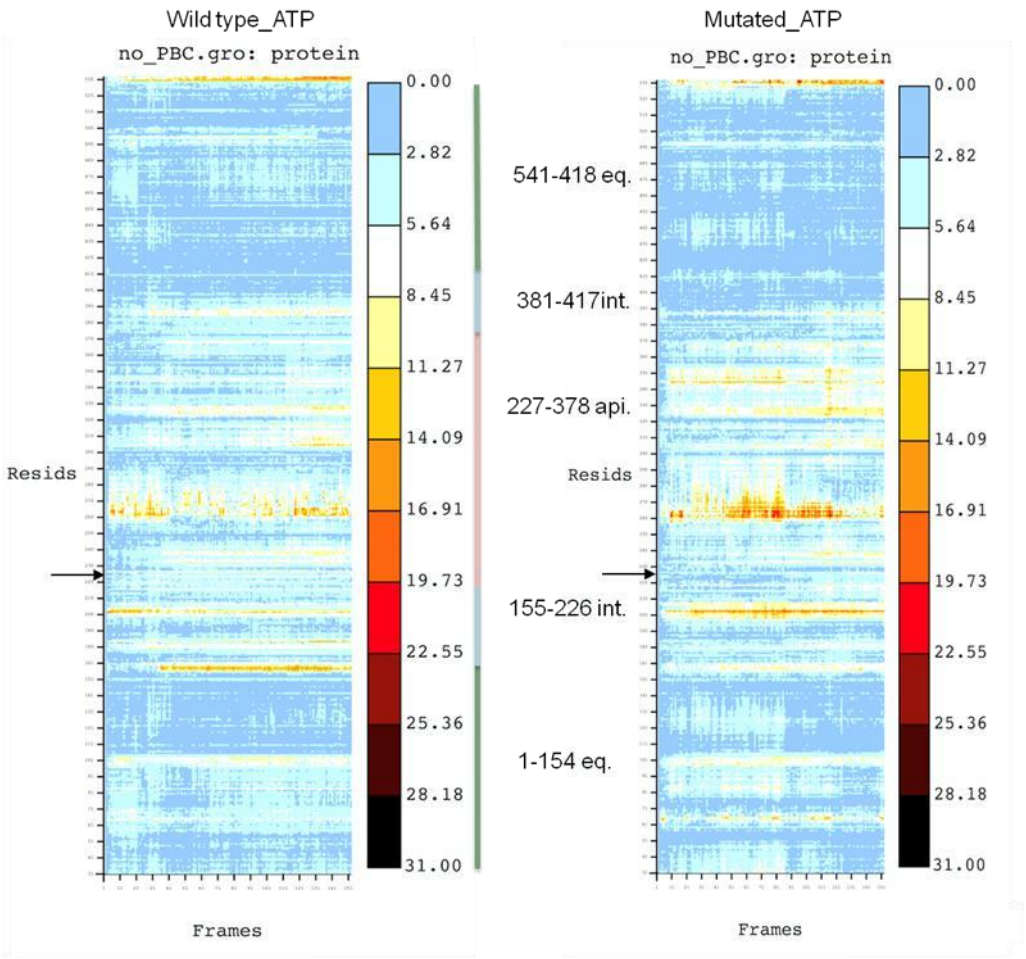

Figure 19

Heat maps of wild type and mutated subunits with ATP: compared to the condition without nucleotide, in the wild type subunit no particular area of heat is detected, while in the mutated, a “redder " area in the apical domain is detected, in accordance with superposition D

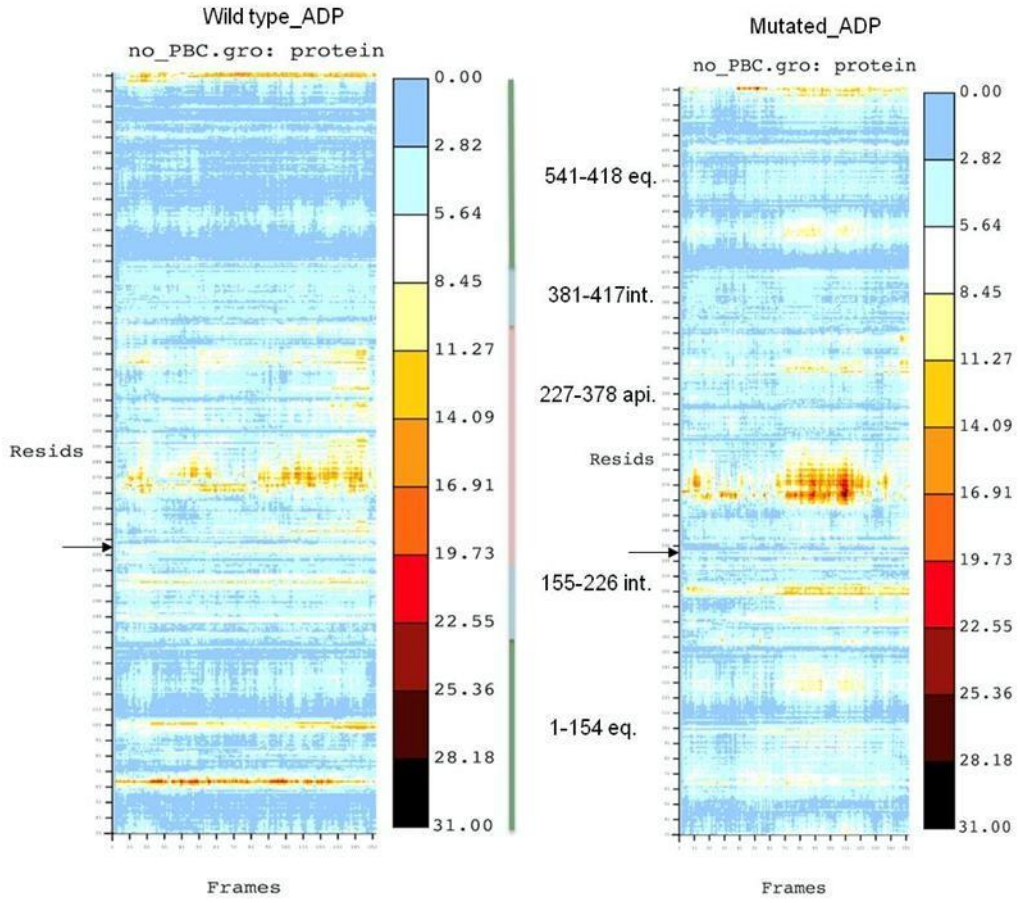

Figure 20

Heat maps of wild type and mutated subunits whit ADP: similar to the ATP-linked situation, the wild type subunit map shows no substantial area of heat, if not at the end of the simulation always in the apical region, while the mutated subunit map shows a wider apical red region but only in a small time interval. This is consistent with the superposition E.

3. *Ex vivo* analysis

3.1 Morphological analysis of mutated tissue

To know the effects of the mutation on skeletal muscle tissue I first performed a hematoxylin-eosin staining (Figure 21).

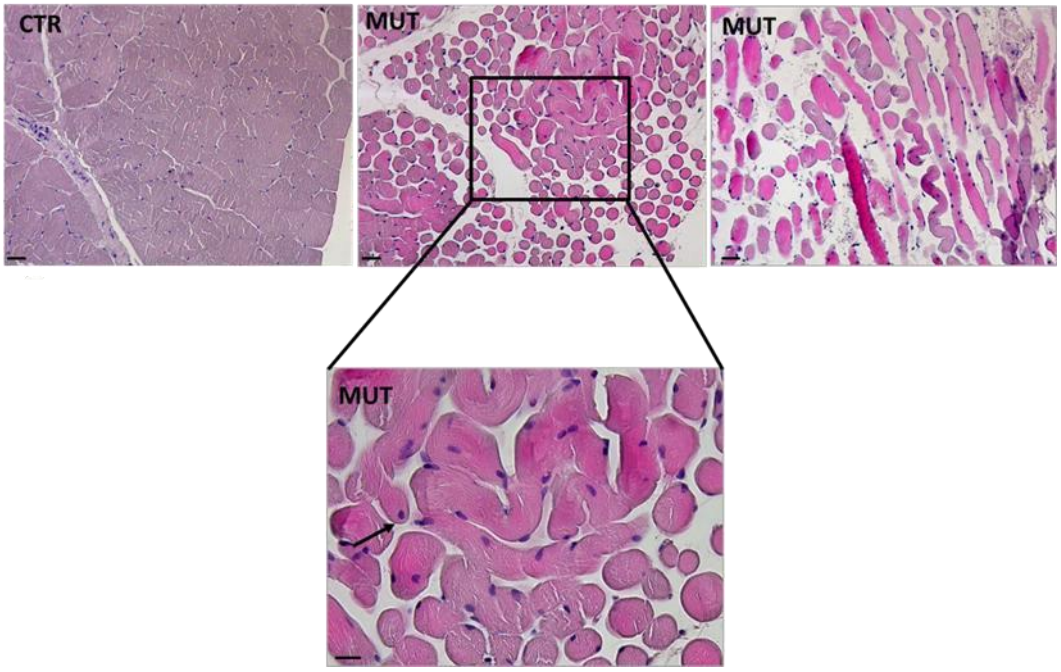

Figure 21

Hematoxilin-eosin on lateral grastrocnemius biopsy from patient (MUT) and healthy skeletal muscle tissue (CTR). Significance changes was observed in mutated tissue compared to the healthy one (Bar=100µM).

The microscopic observation of the mutated skeletal muscle biopsy evidences a widespread atrophic process. The muscle fibers are notably different in shape and size. Most fibers are small and rounded. Focally, the central fibers are enlarged (Figure 22 below).

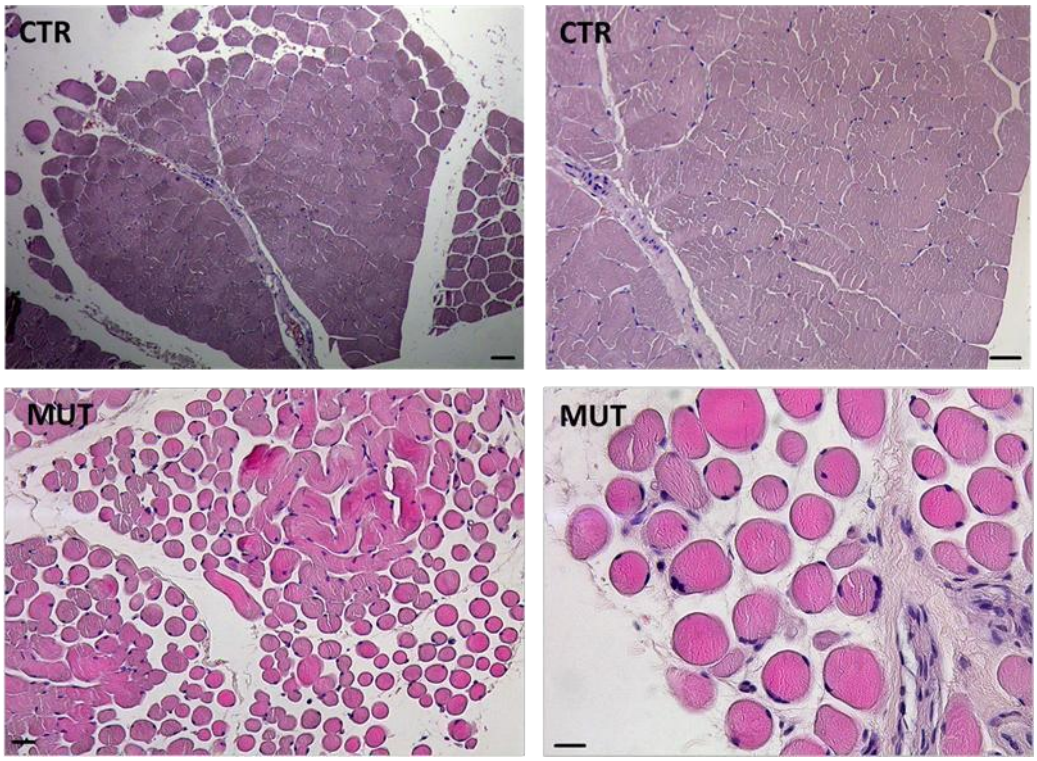

Figure 22

Hematoxilin-eosin stain, skeletal muscle control (CTR) and mutated (MUT). (Bar=100µM)

There is much evidence of wavy fibers that often are hypereosinophilic. The nuclei, in cross section, are pheripheral or subsarcolemmal in most fibers, even if, in 5% percent of fibers, are internal and in paracentral position (arrows in Figure 23 below).

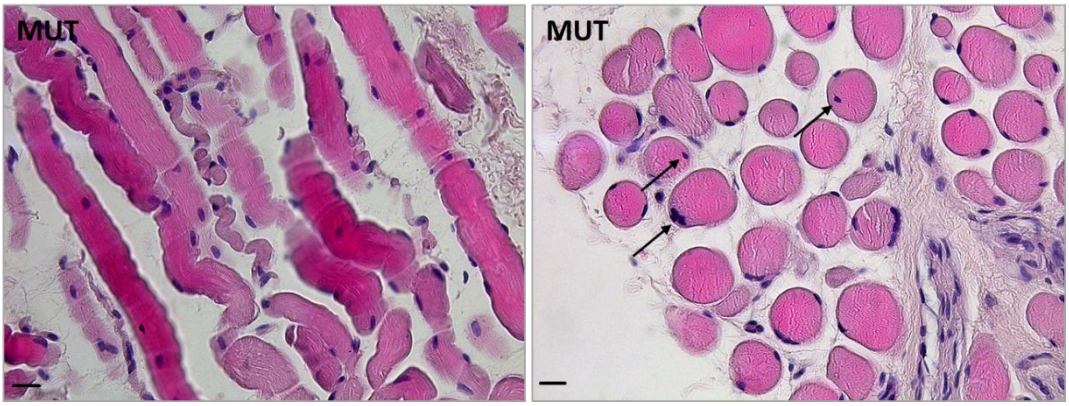

Figure 23

Hematoxilin-eosin stain (Bar=100µM), mutated skeletam muscle (MUT).

The fibers in longitudinal section shown a striated pattern. Most fibers are ring fibers that, in cross sections, shown a striated annulation due to an abnormal orientation of myofibrils. To better reveal the annulation (black arrow in Figure 24 below) an Alcian-Pas staining was performed:

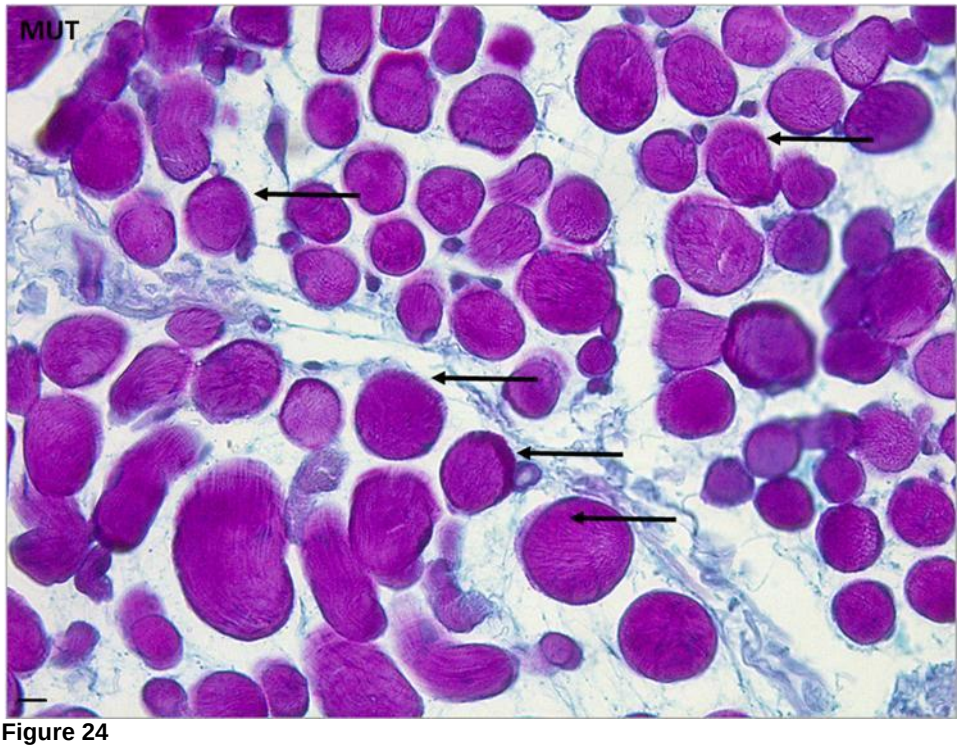

Figure 24

Alcian-Pas staining of mutated skeletal muscle tissue (MUT).

3.2 Assessment of apoptosis in mutated skeletal muscle tissue

To evaluate whether the atrophy observed in the hematoxylin-eosin staining was the result of a cellular apoptosis, a TUNEL assay was performed on the mutated skeletal muscle tissue and on the control tissue (respectively MUT and CTR in Figure 25).

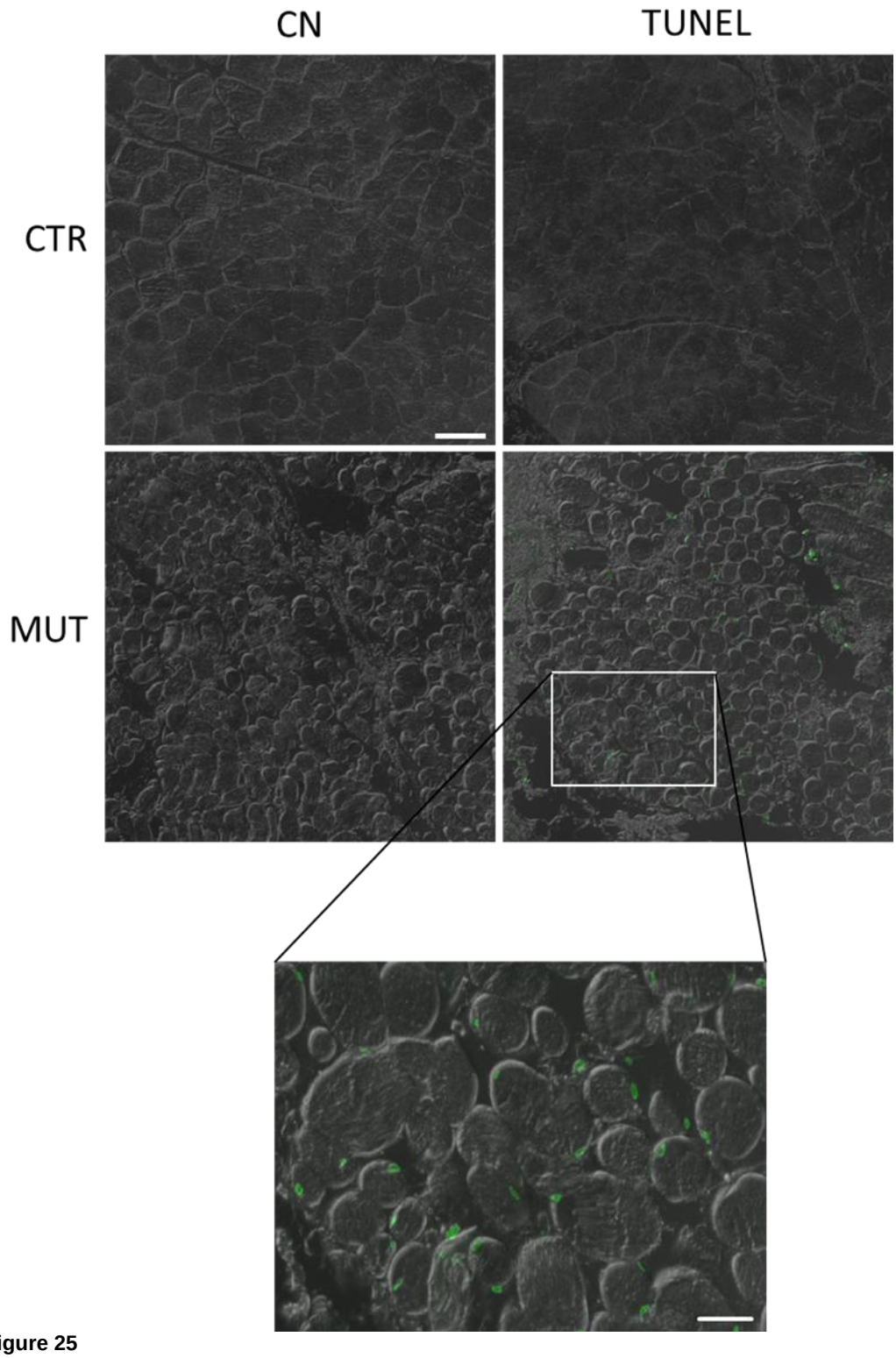

Figure 25

Apoptosis assay. Representative image of TUNEL staining of mutated skeletal muscle tissue (MUT) (Bar = 100 μm).

DNA strand breaks are much more present compared to control tissue.

3.3 Characterization of mutated skeletal muscle tissue by double immunofluorescence analysis (IF)

Double immunofluorescence tests were performed to assess the localization of laminin and Pax7. Samples, mutated and control, were stained for anti-laminin to verify the morphology of skeletal muscle tissue and to evaluate the level and distribution of laminin (Figure 26, green). Laminin of mutated tissue presents typical organization outlining the extracellular membranes of muscle fibers. However, it appears strongly localized into extracellular matrix of mutated tissue.

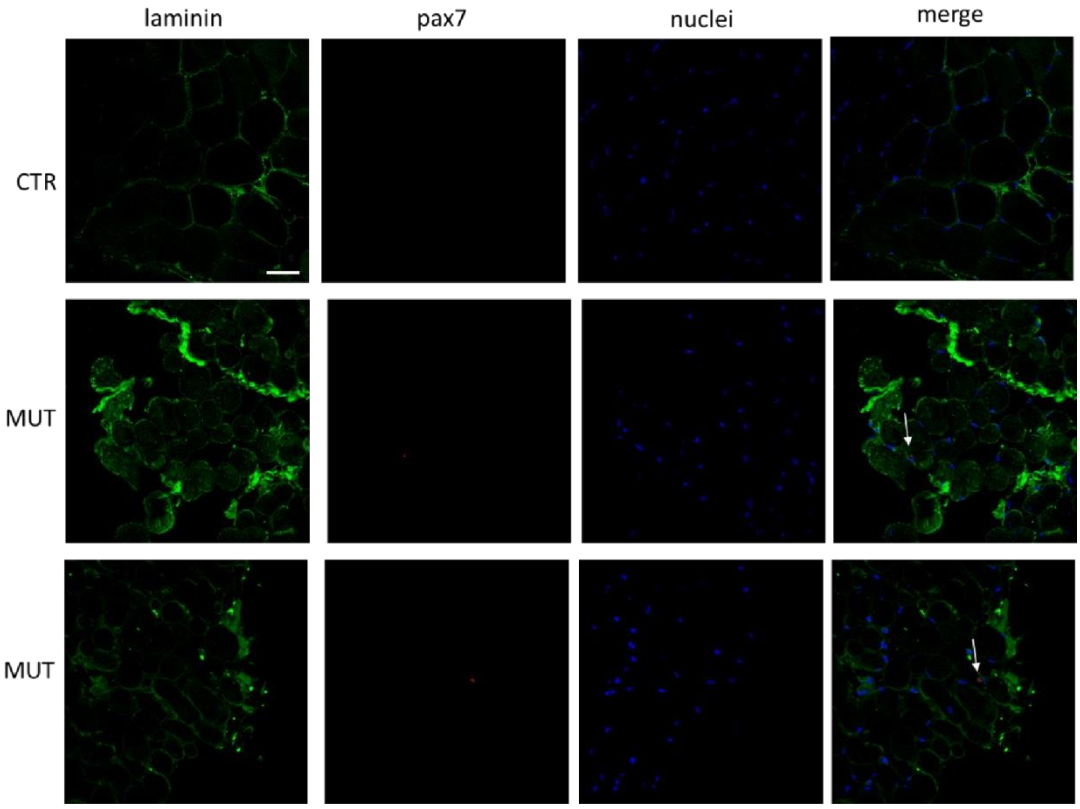

Figure 26

Double immunofluorescence analysis of laminin cellular distribution and pax7 presence in healthy control (CTR) and mutate (MUT) tissues. Both tissue showed laminin positivity in extracellular membrane. A strong extracellular matrix localization of laminin was observed in mutated tissue. Pax7 was detected only in mutated tissue. Pax7 was detected by TRICT conjugated antibody, laminin by a FITC conjugated antibody and nuclei were stained by Hoechst 33342 and fluorescent cells were visualized by a confocal Leica microscope with fluorescent filters for TRICT, FITC and HOECHST respectively. Presence of pax7 is shown by the merge of laminin and nuclei staining (Bar=25µM).

To investigate also the presence of satellite cells the anti-Pax7 was used with anti-laminin antibodies. Control healthy tissue shows only a single

staining, indicating that Pax7 was not present. Instead, in two different fields of the mutated tissue the presence of a satellite cell for each was found (Figure 26 and panels numbers 1 and 2 of Figure 27, in red).

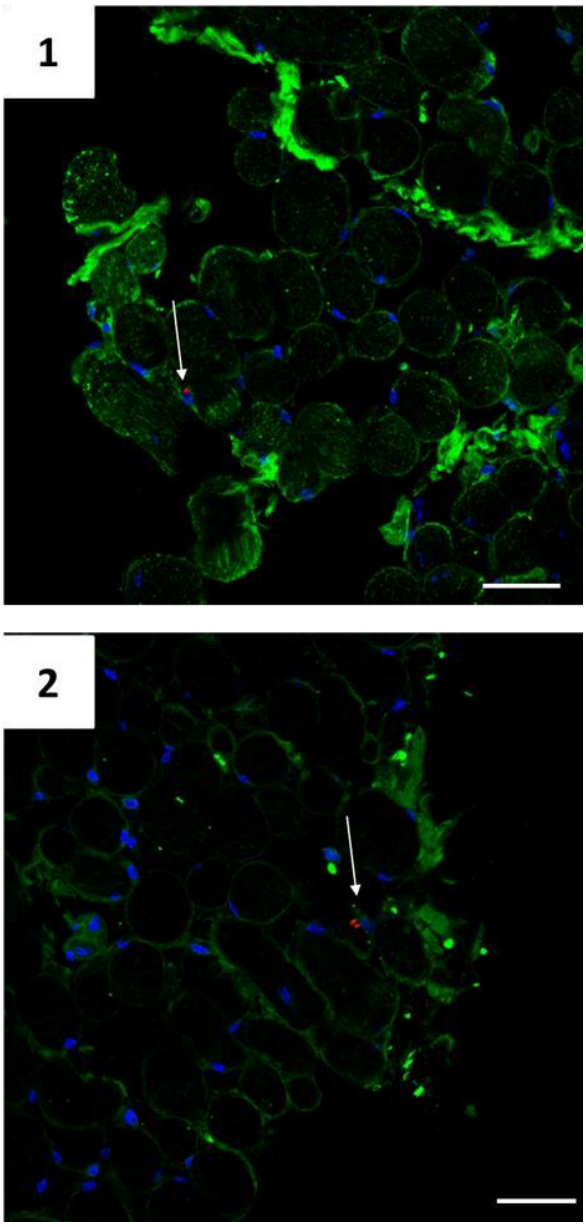

Figure 27

Panel 1 and 2 are magnification merge double immunofluorescence of Figure 26 to better visualize Pax7 positive fibers in mutated skeletal muscle tissue. (FITC, conjugated with anti-laminin antibody; TRITC, conjugated with anti-Pax7 antibody; nuclei with probe HOECHST) Tissues were analysed in a Leica laser scanning confocal microscope (Bar=25µM).

3.4. CCT5 immunofluorescence on human skeletal muscle tissue: presence and localization

Since there are no literature data on the presence and localization of the CCT5 subunit in healthy human skeletal muscle tissue, immunofluorescence for CCT5 subunit was performed on both types of

tissue, wild type and mutated. The localization of CCT5 at the nuclear level was evaluated.

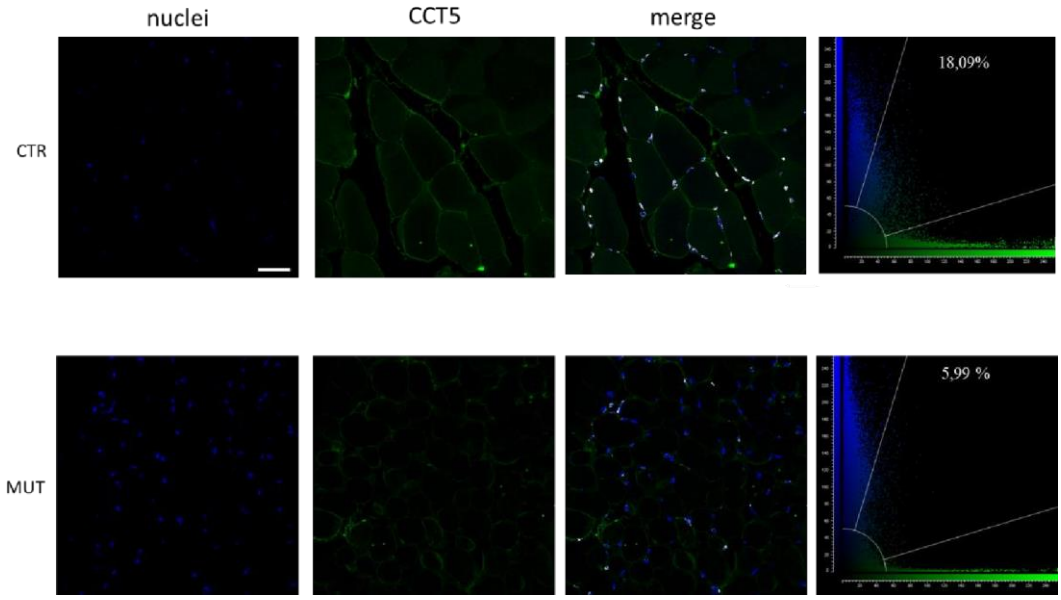

Figure 28

Healthy and mutated skeletal muscle tissues were stained with FITC, conjugated with anti-CCT5 antibody, and with the nuclei probe HOECHST. Tissues were analysed in a Leica laser scanning confocal microscope (Bar = 25 μm).

In healthy human skeletal muscle, CCT5 is located at both cytoplasmic and nuclear levels, while its presence following the L224V mutation appears to be strongly diminished in both intracellular compartments.

The localization rate of nuclear CCT5 is 18.09% and 5.99%, respectively in control skeletal muscle tissue and in mutated skeletal muscle tissue.

3.5 Evaluation of CCT5 mRNA expression

To assess and verify the immunofluorescence results, CCT5 levels in mutated skeletal muscle tissue were performed also by molecular investigations. Total RNA was extracted from pieces of mutated and control skeletal muscle biopsies, RT-PCR was performed using gene-specific primers (Table 7). The expression of this chaperonin was evaluated lower in mutated biopsy confirming the immunofluorescence investigation. Data are not reported because being a unique case report I cannot perform a statistical evaluation with a standard deviation.

3.6 α-actin cell distribution assessment: Immunofluorescence analysis (IF)

Samples were stained for anti-α-actin (Figure 29, green) to verify the cytoskeleton muscle fibers and to study the presence and localization of this protein both in healthy and mutated (respectively, CTR and MUT in Figure 29) tissues. α-actin presents typical organization, compatible with its normal localization, along cytoskeleton and near membrane. Even if its distribution appears normal, it seems that, due to the altered and sigmoid morphology of mutated fibers, the α-actin is not homogeneously present at the point where the fiber changes direction.

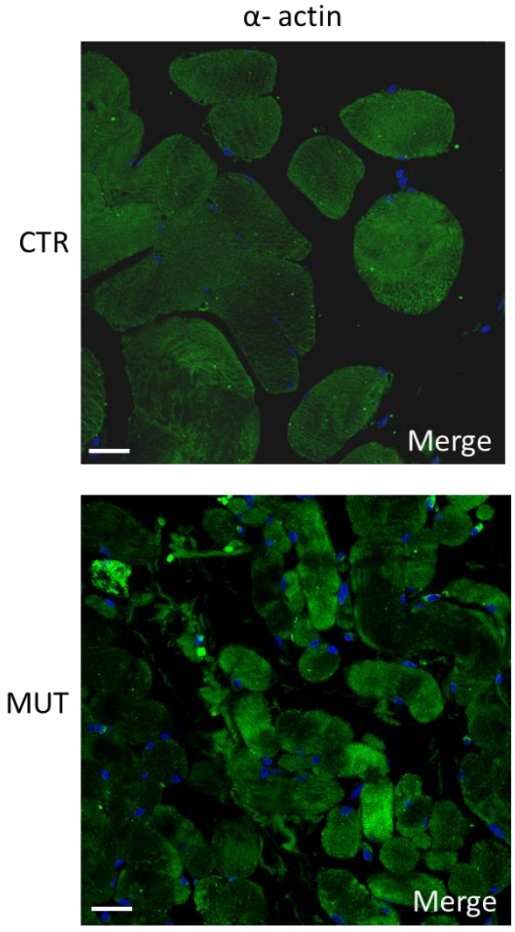

Figure 29

Healthy and mutated skeletal muscle tissues were stained with FITC, conjugated with anti-α-actin antibody, and with the nuclei probe HOECHST. Tissues were analysed in a Leica laser scanning confocal microscope.

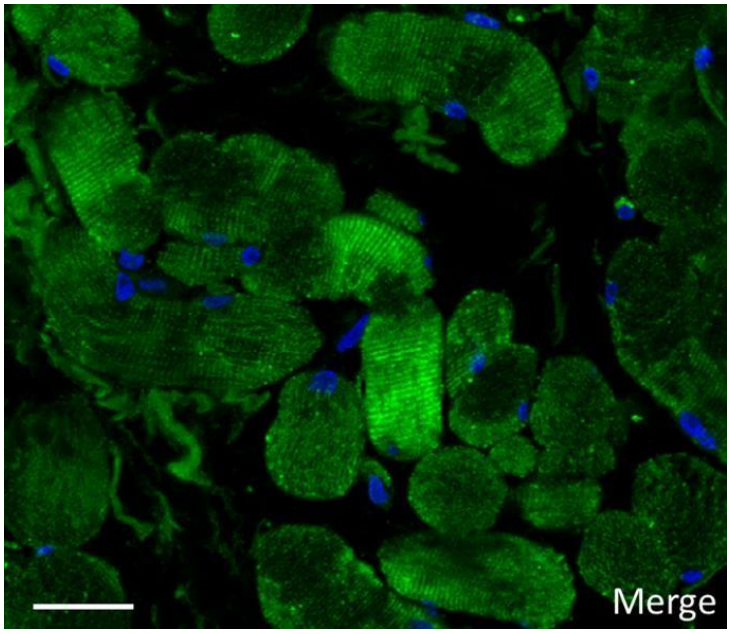

Figure 30

Magnification merge immunofluorescence of Figure 29 to better visualize α-actin in fibers of mutated skeletal muscle tissue. (FITC, conjugated with anti- α-actin antibody; nuclei stained with probe HOECHST) Tissues were analysed in a Leica laser scanning confocal.

Discussion

Investigating rare genetic diseases is a complex challenge due to their frequency and incidence, when is involved the nervous system, the issue becomes more complicated. The study of the nervous tissue, primarly damaged, is very unlikely. For these reasons, knowledges about these diseases are often confusing and sometimes conflicting.

In the family of genetic leukodystrophies have been included several clinical cases which share as pathological hallmark the loss of the white substance, the myelin sheath, which surrounds the axons of neurons. Some of them are caused by mutations on the genes encoding for myelin proteins (myelinopathies), therefore the molecular process is intuitive. However, in other genetic leukodystrophies occur mutations in “non-myelinic” gene and the molecular processes have not yet been identified. Several studies have been shown that mutations on Hsps cause neurodegenerative diseases.

The possibility of classifying these leukodystrophies as chaperonopathies was a further aim in the years of my PhD, not only for a more accurate molecular characterization of the pathologies, but also to warn clinicians in evaluating a mutation on a molecular chaperone gene when the patient shows a leukodystrophic symptomatology not linked to mutations on genes coding for myelin proteins. Therefore, how rare are these diseases truly?

Previous studies have indicated a crucial role of Hsp60 and CCT chaperonins. However, even if the mutations on the chaperonins described cause similar symptomatology, a great heterogeneity is remarkable (Table 9).

Disease Myelin Status Chaperonopathy	Mutation	Genetic Condition	Clinical-Pathological Features	Reference
Peripheral neuropathy Demyelinating By defect	CCT5-p.His147Arg (consanguineous Moroccan family)	HET	Progressive distal sensory neuropathy of upper and lower limbs leading to mutilating acropathy; abnormality of the lipoprotein profile; severe atrophy of the spinal cord predominantly in the posterior tract (MRI).	[6]
SPG13 Possibly demyelinating By defect	Hsp60-p.Val98Ile (French family)	HET [1]	Severe functional handicap; decreased vibration sense; urinary urgency; pes cavus; increased reflexes in the lower and upper limbs; loss of Babinski sign.	[11]
MitCHAP-60 disease Hypomyelinating By defect	Hsp60-p.Asp29Gly (consanguineous Israeli Bedouin kindred)	HOM	Rotatory nystagmus, progressive spastic paraplegia; variable rate of neurological deterioration and regression; severe motor impairment; abnormal head control; profound mental retardation; hypomyelinating leukodystrophy (MRI).	[12]
Asymptomatic or symptomatic	Hsp60-p.Gln461Glu (Danish HSP patients)	HET	Asymptomatic or symptomatic. Symptomatic cases show: spasticity and weakness in the lower limbs and impaired vibration sense in the toes; normal cerebrum and spinal cord MRI; abnormal motor-evoked and somatosensory evoked potentials; evoked potentials (VEP) abnormal on the left eye.	[13]
MitCHAP-60 disease Hypomyelinating By defect	Hsp60-p.Asp29Gly (Syrian boy)	HOM	Slow psychomotor development; absence of heat control; hypotonia; nystagmus; limb spasticity; feeding difficulties; no evidence of normal myelination (MRI)	[14]

[1] Abbreviations: HET, heterozygosity; HOM: homozygosity; MRI, magnetic resonance imaging; HSP: hereditary spastic paraplegia. Note: the list of myelin disorders primarily or secondarily dependent on chaperones that are abnormal due to genetic or acquired defects will most likely increase quite significantly in the near future, if clinicians and pathologists are aware of their existence and look for them.

Table 9

Diseases with myelin abnormality associated with chaperone gene mutations[75]

Understanding the cellular and molecular events responsible for these chaperonopathies is the first and fundamental step towards developing therapeutic solutions like cheperonotherapies.

1. About *in vivo* experiments

On this purpose my PhD project proposed for the first time, the use of zebrafish as suitable model for mimicking human chaperonopaties. Indeed, despite much evidence suggests this non-mammalian vertebrate as powerful tool to study chaperonopathies, there are no reports that directly use the zebrafish model.

To achieve this goal, we have considered to perform CRISPR/Cas9 technique on human orthologous Hsp60 gene of zebrafish, to evaluate V98I point mutation causing SPG13 disease[68].

Preliminary data of this *in vivo* model show that we have not succeeded in isolating a mutated model.

The Surveyor assay I performed in F0 generation allows quick and easy detection of mutations and polymorphisms in DNA.

Despite this assay cannot confirm the presence of the desired mutation, it allows to define the quality of the CRISPR / Cas9 technique.

Analyzing F0 generation we confirmed the successful outcome of the technique by finding indel at the point of the sequence of our interest, however the subsequent analysis of the F1 generation did not confirm a positive outcome, and no fish in heterozygosity was isolated.

The F0 subjected to CRISPR / Cas9, is a “mosaic” generation for the mutation: some somatic cells may have been correctly mutated, but the germ line cells not. Only the analysis of F1 can confirm a germ line transmission of mutation to the offspring.

Five fish belonging to the F1 generation had been isolated as possible "mutation carriers", but mating them with wild type fish, we did not find in their offspring any mutation in heterozygous, as we expected. The mutation does not seem to have been preserved.

This attempt to model the SPG13 in the zebrafish does not want to exclude the possibility that this model is useful to study chaperonopathies. On the contrary, we paved the way for a more conscious approach to modelling chaperonopathies via CRISPR / Cas9 on zebrafish. In fact, some tricks are:

- Development from the embryonic stage to the adult stage of zebrafish requires at least 3 months. Considering the number of embryos to be microinjected to obtain an optimal success rate of the technique and the accuracy of the screening that must be performed on each generation, obtain a stable mutated line in homozygosity requires very long times (prospectively 2 years), excluding the characterization of phenotype through histological and molecular biology analyses.
- The HDR event will happen to a considerable lower frequency than the single indels, if we consider a 30% frequency of indels produced by each

CRISPR, I should expect 9% of frequency for the formation of both indels in the same DNA fragment. Then, this probability should be adjusted for the possible mistakes in the integration of the donor sequence that may considerably lower the chance to find a perfect missense mutation. Monitoring the efficiency of HDR and missense mutation integration in the F0 does not overcome this problem because:

1. It is not known what the genetic balance is in zebrafish, the relation whereby the HSPD1 gene acts as a part of the entire gene in the production of a particular phenotypic character.
2. It is not known a zebrafish phenotype regarding the missense mutation.

We have microinjected about 150 embryos. Thinking about the generational steps necessary to get an homozygous model, and considering that every fish mating produces about 50/100 embryos, the number of fish to be screened and kept on the farm increases exponentially. Many fish, however, died, either due to natural causes, or to stress, or due to the mutation.

Properly micro-injected fish could die before genotypic analysis. V98I mutation, albeit pathogenic in homozygosity in human, could determine the death of the animal model already in heterozygosity. We have therefore finally assessed the possibility of inject zebrafish embryos at different and scaling concentration of corresponding V98I mutated mRNA to 1) better recognize possible phenotypes induced by the mutations 2) find a mRNA work-concentration to define embryos mortality 3) evaluate what may I expect from CRISPR/Cas9 approach.

2. About bioinformatics analysis and *ex vivo* experiments

To date, we are not familiar with all CCT complex client proteins, but we know that proteins with different functions are the "target" of this complex.

Actin and tubulin are the obligate folding substrates and for this reason the mostly studied. Next to these, however, we also find proteins contain the

WD40 motif involving in cell cycle regulation as Cdh1 and Cdc20p[115] (Figure 31).

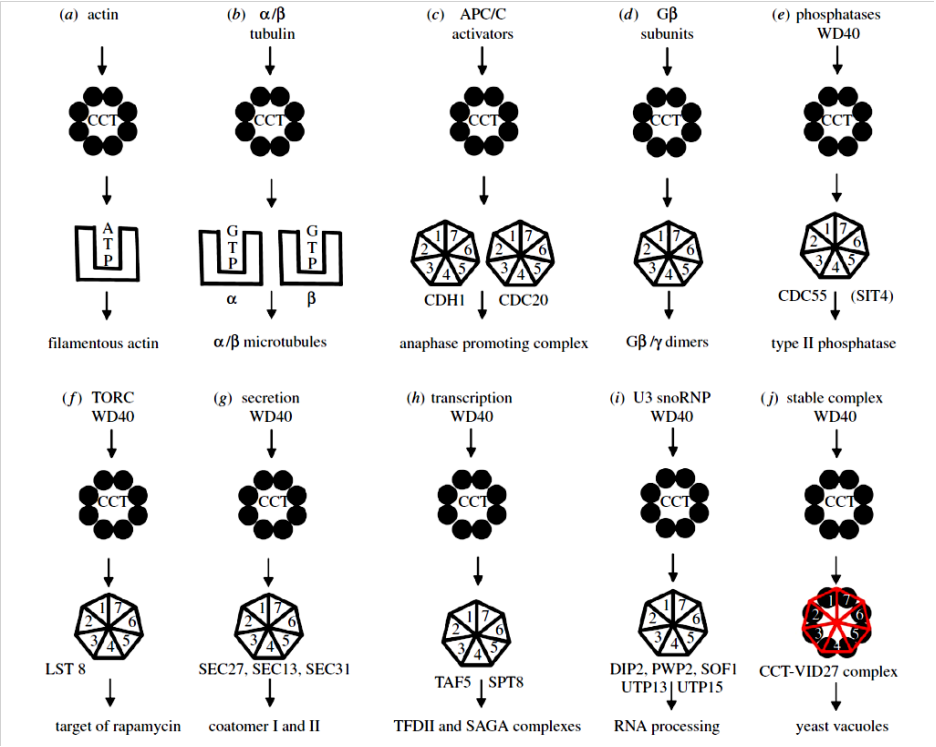

Figure 31

Cartoons of schemes for CCT action upon its substrates and binding complex formation[115].

Other proteins are under investigations as VHL tumor supressor protein[116], huntingtin and α-synuclein protein.

The involvement of the CCT complex in human pathologies is in fact varied and underlies different cellular processes within distinct tissue[117]. It has discovered involved in retinal dystrophy[118], myocardial infarction[119] and dysfunction[120], sensory neuropathy[78], Parkinson's disease[121], and Huntington's disease[122,123].

The importance of studying the functionality of this complex therefore has a very broad spectrum.

Previously reporter H147R mutation occurs in equatorial domain of CCT5 subunit of CCT complex and is related to a peripheral neuropathy with demyelinating and mutilating characteristic[68]. Having analysed a new mutation not yet described in the literature, even in the case of the CCT

complex, we can confirm that different mutations on the same subunit cause a similar but not equal pathology. The patient in whom the new mutation was found has neurodegenerative features but is not mutilating, until now. In addition to traits listed in 2.1 Results section, it is important to emphasize some clinical features that match with leukodystrophy disease: under MRI brain analysis the white matter of posterior regions appears damaged; studies of motor nerve conduction confirm delayed or absent conduction due to a demyelinating neuropathy.

The studies that have been carried out helped to characterize the mutation and to understand if this could really be the cause of CCT complex malfunctioning and, therefore, causes the pathology.

The mutational analysis performed by the software confirm that the mutation has a deleterious and pathological outcome.

The mutation is a point mutation, a substitution of a Leucine with a Valine at position 224. The two amino acids are both non-polar so the physical and chemical characteristics should be maintained. The main element that engaged our interest was a subtle but decisive steric hindrance of Valine in the mutated subunit.

Position 224 within the CCT5 subunit is found in the intermediate domain. This domain apparently does not play a particular function, such as the apical or equatorial domain do. Bioinformatics modelling and radius of gyration analysis show that in all the conditions in which the subunit could be within the complex, (free from any nucleotide bound, linked to ATP or linked to ADP) the mutated CCT5 subunit does not completely overlap the wild type subunit. In particular:

- greater structural incompatibility is found in the condition in the absence of nucleotide
- the domain that is particularly affected by this mutation is the entire apical domain

It therefore seems that the mutation at position 224 of CCT5 subunit intermediate domain somehow causes a sort of resonance effect on the apical domain. It could upsetting the balance of the whole complex, during

the aggregation processes of the eight subunits and/or during the recognition and folding of client proteins.

The mutated subunit modelling showed a larger discrepancy with wild type modelling subunit. More in-depth analysis of RMSD defines that:

1. CCT5 subunit appears not be in the same anatomical conformation in all three conditions.
2. The first string encoding for intermediate domain, where the mutation takes place, suffers mainly the aminoacidic change.
3. There is a great instability of apical domain: resonance effect.

All other domains not presented relevant developments.

Heat maps of the mutated CCT5 subunit confirm the instability of the apical domain corresponding to helix-10, proximal loop and helix-9 position in the absence of nucleotide. The CCT5 subunit in literature is described as the subunit that is particularly involved in the hydrolysis of ATP within the complex rather than in binding to substrate proteins[114]. Indeed, H147R mutation demonstrate its important function.

Therefore, we would not have expected a decisive involvement of the L224V mutation which affects “per resonance” the apical domain. We could hypothesize that the CCT5 protein plays a fundamental role even with its apical domain.

Several studies demonstrated that CCT complex binds different substrates *in vitro* or *in vivo*. *In vitro* studies suggested that CCT chose its client proteins if they presented a specific sequence motif. Actually, CCT makes an even more accurate selection of binding proteins influenced by the translational context in which it is present[124]. Thus, in different tissues (with different proteome), in different conditions (e.g. stress condition), it can bind different substrates. Mutated CCT can afflict or not, strongly or slightly, specific processes and cause typical damage to the tissue.

The mutation L224V afflicts human skeletal muscle tissue. Histological analysis of human mutated skeletal muscle tissue shows a strong atrophic

process with a conspicuous deposition of extracellular matrix. Fibers appear disorganized and morphologically anomalous in shape and size.

The results obtained with TUNEL assay show that muscle atrophy is not caused by a necrosis that could be linked to a denervation of the fibers. The L224V mutation has its severe pathogenic effect even within the skeletal muscle tissue.

Despite impairment, the tissue remodelling active attempt is demonstrated by the presence of positive Pax7 cells. This agrees with what is shown in the hematoxylin-eosin staining, in which, although low, a percentage of paracentric nuclei was present within the fibers. CCT plays an important role modulating apoptosis[125]. It regulates the Stat3 folding and ensures its functionality within the cell[125].

Stat3 is a multidomain transcription factor which transmits the signal from cells surface to the nucleus due to the binding with over 40 peptide hormones, therefore it is involved in many cellular pathways including apoptosis[125]. An enhancement of Stat3 has been shown prevent apoptosis of parenchymal cells within different organs[126,127]. Moreover, TRiC binds and promotes the protein folding of p53[128] which in addition to being a tumor suppressor protein, it also modulates the expression of a variety of genes involved in cellular responses such as cell-cycle arrest and apoptosis[129].

Regarding the state of apoptosis of the mutated tissue we can hypothesize that a failure of the CCT function does not allow a correct balance of the anti and pro apoptotic signals necessary for cellular homeostasis.

Throughout immunofluorescence experiments I demonstrate that subcellular localization of CCT5 subunit in human skeletal muscle cells is both nuclear and cytoplasmic. No previous literature data reported this notice. The knowledge about the subcellular localization was useful to identify if there was a different localization and expression of the CCT5 subunit within the affected tissue. In addition to a lower cytoplasmic localization, the mutated tissue showed a nuclear colocalization of the CCT5 subunit less than 1/3 compared to healthy tissue. The lower

expression of the CCT5 subunit was also confirmed by molecular biology data: a substantial minor amplification of the gene had been detected by PCR. These data coincide with the hypothesis that a lower expression of the CCT5 subunit can lead to a diminished presence of the entire CCT complex and therefore a dysfunction of the processes managed by it, such as apoptosis.

To further elucidate the involvement of mutated CCT5 subunits in organization of cytoskeleton proteins I performed immunofluorescence to evaluate α-actin, one of CCT complex main substrate, and laminin.

Data on cytoskeletal proteins, seem to show that the mutation creates a poorly homogeneous distribution of α-actin filaments highlighting a sort of interruption of the filaments especially in fiber central spot or when the fiber changes direction. Laminin, on the other hand, appears to be rather present mainly in the extracellular environment.

Based on what we know, we expected greater cytoskeletal dysfunction.

However, as mentioned above, the (wild type or mutated) CCT complex can affect specific cellular processes based on the transcriptome context in which it is found. Furthermore, protein substrates are often folded by different and several molecular chaperones or chaperonins. For example, the small heat shock protein Hsp27 plays a role in diverse cellular processes, including cellular stress response, protein chaperone activity, regulation of cellular glutathione levels, apoptotic signaling, and finally in regulation, polymerization and stability of actin, in cardiac and skeletal muscle cells[130].

Therefore, we cannot exclude that a compensation process may exist within the cells[130]. Hsp27 e.g., it could also partially offset the CCT dysfunction, concerning the stability of actin filaments. Furthermore, mutation in Hsp27 has been related to the human congenital neuropathy Charcot-Marie Tooth (CMT) disease[131].

Final remarks

To summarise the data obtained and described in this thesis, I have found that it is necessary to know the genetic balance of HSPD1 gene on

zebrafish before starting with DNA editing technique to recognize a possible phenotype.

Different mutations occurring in the same protein can manifest themselves diversely at molecular level, and furthermore, cause different pathologies. Bioinformatic analysis demonstrate that a mutation which occurs in a position within a protein can, by resonance, show its effect in a farthest site of the same protein, thus modifying its activity.

The new mutation in CCT5 subunit cause neurodegenerative disease as symptomatologic described. Histological analysis demonstrates a damaged human skeletal muscle tissue due to L224V mutation. Therefore, muscle damage does not appear to be a secondary effect of nervous deterioration.

Nevertheless, nervous tissue is the most damaged one. This would suggest a greater susceptibility to the tissue. Further studies are needed to define the cellular cytotype mainly involved, however the investigations reported to date which consider the involvement of chaperonins in neurodegenerative disease, report myelin deterioration. According to neurological examinations of the new case here discussed, myelin is impaired. It is not to be excluded that the L224V mutation on CCT5 also causes a failure of the myelin sheet around the axons of neurons.

Furthermore, we show that CCT5 is expressed in cytosol and nucleus of muscle fibers, data not yet reported in the literature. Due to L224V mutation CCT5 is poorly localized and expressed in both compartments.

Taken together these observations and results suggested that knowing the molecular processes that underlie chaperonins and molecular chaperones is an important goal for developing new therapeutic approaches.

References

1. Gray's Atlas of Anatomy - 1st Edition. Available at: https://www.elsevier.com/books/grays-atlas-of-anatomy/drake/978-0-443-06721-1. (Accessed: 13th November 2019)
2. Neuroanatomia Funzionale -. Available at: https://www.idelsongnocchi.com/prodotto/neuroanatomia-funzionale/. (Accessed: 13th November 2019)
3. Bavisotto, C. C. *et al.* Extracellular vesicle-mediated cell–cell communication in the nervous system: Focus on neurological diseases. *International Journal of Molecular Sciences* **20**, (2019).
4. Allen, N. J. & Barres, B. A. Neuroscience: Glia - more than just brain glue. *Nature* **457**, 675–677 (2009).
5. Azevedo, F. A. C. *et al.* Equal numbers of neuronal and nonneuronal cells make the human brain an isometrically scaled-up primate brain. *J. Comp. Neurol.* **513**, 532–541 (2009).
6. Janowska, J. *et al.* Directed glial differentiation and transdifferentiation for neural tissue regeneration. *Experimental Neurology* **319**, (2019).
7. Jäkel, S. & Dimou, L. Glial cells and their function in the adult brain: A journey through the history of their ablation. *Frontiers in Cellular Neuroscience* **11**, (2017).
8. Hoogland, T. M. & Kuhn, B. Recent developments in the understanding of astrocyte function in the Cerebellum in vivo. *Cerebellum* **9**, 264–271 (2010).
9. Shemer, A. & Jung, S. Differential roles of resident microglia and infiltrating monocytes in murine CNS autoimmunity. *Seminars in Immunopathology* **37**, 613–623 (2015).
10. Hickman, S., Izzy, S., Sen, P., Morsett, L. & El Khoury, J. Microglia in neurodegeneration. *Nature Neuroscience* **21**, 1359–1369 (2018).
11. Lee, Y. il, Thompson, W. J. & Harlow, M. L. Schwann cells participate in synapse elimination at the developing neuromuscular junction. *Current Opinion in Neurobiology* **47**, 176–181 (2017).
12. Hanani, M. Satellite glial cells: More than just rings around the neuron. *Neuron Glia Biology* **6**, 1–2 (2010).
13. Myasthenia Gravis and Other Diseases of the Neuromuscular Junction | Harrison's Principles of Internal Medicine, 20e | AccessMedicine | McGraw-Hill Medical. Available at: https://accessmedicine.mhmedical.com/content.aspx?bookid=2129&sectionid=192533554. (Accessed: 13th November 2019)
14. Kevelam, S. H. *et al.* Update on leukodystrophies: A historical perspective and adapted definition. *Neuropediatrics* **47**, 349–354 (2016).
15. Bielschowsky, M. & Henneberg, R. Über Bau und Histogenese der zentralen Ganglioglioneurome. *Eur. Neurol.* **68**, 21–51 (1928).
16. Hudson, L. D., Puckett, C., Berndt, J., Chan, J. & Gencic, S. Mutation of the proteolipid protein gene PLP in a human X chromosome-linked myelin disorder. *Proc. Natl. Acad. Sci. U. S. A.* **86**, 8128–8131 (1989).
17. Polten, A. *et al.* Molecular basis of different forms of metachromatic leukodystrophy. *N. Engl. J. Med.* **324**, 18–22 (1991).
18. Kaul, R., Gao, G. P., Balamurugan, K. & Matalon, R. Canavan disease: molecular

basis of aspartoacylase deficiency. *J. Inherit. Metab. Dis.* **17**, 295–7 (1994).

19. Sakai, N. *et al.* Krabbe disease: Isolation and characterization of a full-length cDNA for human galactocerebrosidase. *Biochem. Biophys. Res. Commun.* **198**, 485–491 (1994).

20. Mosser, J. *et al.* Putative X-linked adrenoleukodystrophy gene shares unexpected homology with ABC transporters. *Nature* **361**, 726–730 (1993).

21. Bonkowsky, J. L. *et al.* The burden of inherited leukodystrophies in children. *Neurology* **75**, 718–725 (2010).

22. Ng, S. B. *et al.* Targeted Capture and Massicely Parallel Sequencing of twelve human exomes. *Nature* **461**, 272–276 (2010).

23. Rademakers, R. *et al.* Mutations in the colony stimulating factor 1 receptor (CSF1R) gene cause hereditary diffuse leukoencephalopathy with spheroids. *Nat. Genet.* **44**, 200–205 (2012).

24. Steenweg, M. E. *et al.* Leukoencephalopathy with thalamus and brainstem involvement and high lactate 'LTBL' caused by EARS2 mutations. *Brain* **135**, 1387–1394 (2012).

25. Simons, C. *et al.* A de novo mutation in the β-tubulin gene TUBB4A results in the leukoencephalopathy hypomyelination with atrophy of the basal ganglia and cerebellum. *Am. J. Hum. Genet.* **92**, 767–773 (2013).

26. van der Knaap, M. S., Valk, J., de Neeling, N. & Nauta, J. J. P. Pattern recognition in magnetic resonance imaging of white matter disorders inchildren and young adults. *Neuroradiology* **33**, 478–493 (1991).

27. Parikh, S. *et al.* A clinical approach to the diagnosis of patients with leukodystrophies and genetic leukoencephelopathies. *Molecular Genetics and Metabolism* **114**, 501–515 (2015).

28. Macario, A. J. L. & de Macario, E. C. Sick Chaperones, Cellular Stress, and Disease. *N. Engl. J. Med.* (2005). doi:10.1056/nejmra050111

29. Macario, A. J. L. & Conway de Macario, E. Molecular chaperones: multiple functions, pathologies, and potential applications. *Front. Biosci.* **12**, 2588–600 (2007).

30. Voellmy, R. Transduction of the stress signal and mechanisms of transcriptional regulation of heat shock/stress protein gene expression in higher eukaryotes. *Crit. Rev. Eukaryot. Gene Expr.* **4**, 357–401 (1994).

31. Walsh, D. *et al.* The role of heat shock proteins in mammalian differentiation and development. *Environ. Med.* **43**, 79–87 (1999).

32. Murshid, A., Gong, J. & Calderwood, S. K. The role of heat shock proteins in antigen cross presentation. *Front. Immunol.* **3**, 63 (2012).

33. Prohászka, Z. & Füst, G. Immunological aspects of heat-shock proteins-the optimum stress of life. *Mol. Immunol.* **41**, 29–44 (2004).

34. Czarnecka, a M., Campanella, C., Zummo, G. & Cappello, F. Mitochondrial chaperones in cancer: from molecular biology to clinical diagnostics. *Cancer Biol Ther* **5**, 714–720 (2006).

35. Macario, A. J. L., Cappello, F., Zummo, G. & Conway de Macario, E. Chaperonopathies of senescence and the scrambling of interactions between the chaperoning and the immune systems. *Ann. N. Y. Acad. Sci.* **1197**, 85–93 (2010).

36. Garrido, C., Gurbuxani, S., Ravagnan, L. & Kroemer, G. Heat shock proteins: endogenous modulators of apoptotic cell death. *Biochem. Biophys. Res.*

Commun. **286**, 433–42 (2001).

37. Calderwood, S. K., Mambula, S. S. & Gray, P. J. Extracellular heat shock proteins in cell signaling and immunity. *Ann. N. Y. Acad. Sci.* **1113**, 28–39 (2007).

38. Kampinga, H. H. *et al.* Guidelines for the nomenclature of the human heat shock proteins. *Cell Stress Chaperones* **14**, 105–11 (2009).

39. Search | HUGO Gene Nomenclature Committee.

40. Usefulness of the hsp60 gene for the identification and classification of Gram-negative anaerobic rods. - PubMed - NCBI.

41. Campanella, C. *et al.* A comparative analysis of the products of GROEL-1 gene from Chlamydia trachomatis serovar D and the HSP60 var1 transcript from Homo sapiens suggests a possible autoimmune response. *Int. J. Immunogenet.* **36**, 73–8 (2009).

42. Pace, A. *et al.* Hsp60, a novel target for antitumor therapy: structure-function features and prospective drugs design. *Curr. Pharm. Des.* **19**, 2757–64 (2013).

43. Cappello, F. *et al.* Hsp60 chaperonopathies and chaperonotherapy: targets and agents. *Expert Opin. Ther. Targets* **18**, 185–208 (2014).

44. Cappello, F. *et al.* Hsp60 and human aging: Les liaisons dangereuses. *Front. Biosci. (Landmark Ed.* **18**, 626–37 (2013).

45. Flohé, S. B. *et al.* Human heat shock protein 60 induces maturation of dendritic cells versus a Th1-promoting phenotype. *J. Immunol.* **170**, 2340–8 (2003).

46. Ausiello, C. M. *et al.* 60-kDa heat shock protein of Chlamydia pneumoniae promotes a T helper type 1 immune response through IL-12/IL-23 production in monocyte-derived dendritic cells. *Microbes Infect.* **8**, 714–720 (2006).

47. Tomasello, G. *et al.* Changes in immunohistochemical levels and subcellular localization after therapy and correlation and colocalization with CD68 suggest a pathogenetic role of Hsp60 in ulcerative colitis. *Appl. Immunohistochem. Mol. Morphol.* **19**, 552–61 (2011).

48. Cappello, F. *et al.* Convergent sets of data from in vivo and in vitro methods point to an active role of Hsp60 in chronic obstructive pulmonary disease pathogenesis. *PLoS One* **6**, e28200 (2011).

49. Chaston, J. J. *et al.* Structural and Functional Insights into the Evolution and Stress Adaptation of Type II Chaperonins. *Structure* **24**, 364–374 (2016).

50. Pereira, J. H. *et al.* Structure of the human TRiC/CCT Subunit 5 associated with hereditary sensory neuropathy. *Sci. Rep.* **7**, (2017).

51. Lopez, T., Dalton, K. & Frydman, J. The Mechanism and Function of Group II Chaperonins. *Journal of Molecular Biology* **427**, 2919–2930 (2015).

52. Macario, A. J. L. Heat-shock proteins and molecular chaperones: implications for pathogenesis, diagnostics, and therapeutics. *International Journal of Clinical & Laboratory Research* **25**, 59–70 (1995).

53. Soti, C. & Csermely, P. Chaperones come of age. *Cell Stress Chaperones* **7**, 186–90 (2002).

54. Macario, A. J. L., Conway de Macario, E. & Cappello, F. *The chaperonopathies : diseases with defective molecular chaperones*. (Springer, 2013).

55. Hay, D. G. *et al.* Progressive decrease in chaperone protein levels in a mouse model of Huntington's disease and induction of stress proteins as a therapeutic approach. *Hum. Mol. Genet.* **13**, 1389–1405 (2004).

56. Rappa, F. *et al.* HSP-molecular chaperones in cancer biogenesis and tumor therapy: an overview. *Anticancer Res.* **32**, 5139–50 (2012).

57. Magen, D. *et al.* Mitochondrial Hsp60 Chaperonopathy Causes an Autosomal-Recessive Neurodegenerative Disorder Linked to Brain Hypomyelination and Leukodystrophy. *Am. J. Hum. Genet.* **83**, 30–42 (2008).

58. Bugiani, M. *et al.* GJA12 mutations in children with recessive hypomyelinating leukoencephalopathy. *Neurology* **67**, 273–279 (2006).

59. Henneke, M. *et al.* GJA12 mutations are a rare cause of Pelizaeus-Merzbacher-like disease. *Neurology* **70**, 748–754 (2008).

60. Torii, T., Miyamoto, Y., Yamauchi, J. & Tanoue, A. Pelizaeus-Merzbacher disease: Cellular pathogenesis and pharmacologic therapy. *Pediatr. Int.* **56**, 659–666 (2014).

61. Bross, P. & Fernandez-Guerra, P. Disease-associated mutations in the HSPD1 gene encoding the large subunit of the mitochondrial HSP60/HSP10 chaperonin complex. *Frontiers in Molecular Biosciences* **3**, (2016).

62. Horwich, A. L., Fenton, W. A., Chapman, E. & Farr, G. W. Two Families of Chaperonin: Physiology and Mechanism. *Annu. Rev. Cell Dev. Biol.* **23**, 115–145 (2007).

63. Fink, J. K. Hereditary spastic paraplegia. *Curr. Neurol. Neurosci. Rep.* **6**, 65–76 (2006).

64. DeLuca, G. C., Ebers, G. C. & Esiri, M. M. The extent of axonal loss in the long tracts in hereditary spastic paraplegia. *Neuropathol. Appl. Neurobiol.* **30**, 576–584 (2004).

65. Blackstone, C. Converging cellular themes for the hereditary spastic paraplegias. *Current Opinion in Neurobiology* **51**, 139–146 (2018).

66. Crosby, A. H. & Proukakis, C. Is the transportation highway the right road for hereditary spastic paraplegia? *Am. J. Hum. Genet.* **71**, 1009–1016 (2002).

67. Bross, P., Rugarli, E. I., Casari, G. & Langer, T. Protein quality control in mitochondria and neurodegeneration in hereditary spastic paraplegia. in 97–121 (2004). doi:10.1007/b95865

68. Hansen, J. J. *et al.* Hereditary spastic paraplegia SPG13 is associated with a mutation in the gene encoding the mitochondrial chaperonin Hsp60. *Am. J. Hum. Genet.* **70**, 1328–1332 (2002).

69. Bross, P. *et al.* The Hsp60-(p.V98I) mutation associated with hereditary spastic paraplegia SPG13 compromises chaperonin function both in vitro and in vivo. *J. Biol. Chem.* **283**, 15694–15700 (2008).

70. Hansen, J. *et al.* A novel mutation in the HSPD1 gene in a patient with hereditary spastic paraplegia. *J. Neurol.* **254**, 897–900 (2007).

71. D'Amico, A. *et al.* Incomplete penetrance in an SPG3A-linked family with a new mutation in the atlastin gene. *Neurology* **62**, 2138–2139 (2004).

72. Bürger, J. *et al.* Hereditary spastic paraplegia caused by mutations in the SPG4 gene. *Eur. J. Hum. Genet.* **8**, 771–776 (2000).

73. Miyamoto, Y. *et al.* Data supporting mitochondrial morphological changes by SPG13-associated HSPD1 mutants. *Data Br.* **6**, 482–488 (2016).

74. Miyamoto, Y. *et al.* Hypomyelinating leukodystrophy-associated missense mutation in HSPD1 blunts mitochondrial dynamics. *Biochem. Biophys. Res. Commun.* **462**, 275–281 (2015).

75. Scalia, F., Marino Gammazza, A., Conway de Macario, E., Macario, A. J. L. & Cappello, F. Myelin Pathology: Involvement of Molecular Chaperones and the Promise of Chaperonotherapy. *Brain Sci.* **9**, 297 (2019).

76. Min, W. *et al.* A human CCT5 gene mutation causing distal neuropathy impairs hexadecamer assembly in an archaeal model. *Sci. Rep.* **4**, (2014).

77. Sergeeva, O. A., Tran, M. T., Haase-Pettingell, C. & King, J. A. Biochemical characterization of mutants in chaperonin proteins CCT4 and CCT5 associated with hereditary sensory neuropathy. *J. Biol. Chem.* **289**, 27470–27480 (2014).

78. Pereira, J. H. *et al.* Structure of the human TRiC/CCT Subunit 5 associated with hereditary sensory neuropathy. *Sci. Rep.* **7**, 3673 (2017).

79. Hein, M. Y. *et al.* A Human Interactome in Three Quantitative Dimensions Organized by Stoichiometries and Abundances. *Cell* **163**, 712–723 (2015).

80. Fink, J. K. Hereditary spastic paraplegia: Clinico-pathologic features and emerging molecular mechanisms. *Acta Neuropathologica* **126**, 307–328 (2013).

81. Kinth, P., Mahesh, G. & Panwar, Y. Mapping of zebrafish research: A global outlook. *Zebrafish* **10**, 510–517 (2013).

82. Grunwald, D. J., Kimmel, C. B., Westerfield, M., Walker, C. & Streisinger, G. A neural degeneration mutation that spares primary neurons in the zebrafish. *Dev. Biol.* **126**, 115–128 (1988).

83. Haffter, P. *et al.* Mutations affecting pigmentation and shape of the adult zebrafish. *Roux's Arch. Dev. Biol.* **206**, 260–276 (1996).

84. Nasevicius, A. & Ekker, S. C. Effective targeted gene 'knockdown' in zebrafish. *Nat. Genet.* **26**, 216–220 (2000).

85. Balciuniene, J. *et al.* Efficient disruption of Zebrafish genes using a Gal4-containing gene trap. *BMC Genomics* **14**, 619 (2013).

86. Hwang, W. Y. *et al.* Efficient genome editing in zebrafish using a CRISPR-Cas system. *Nat. Biotechnol.* **31**, 227–229 (2013).

87. Auer, T. O., Duroure, K., De Cian, A., Concordet, J. P. & Del Bene, F. Highly efficient CRISPR/Cas9-mediated knock-in in zebrafish by homology-independent DNA repair. *Genome Res.* **24**, 142–153 (2014).

88. Malafoglia, V. *et al.* Extreme thermal noxious stimuli induce pain responses in zebrafish larvae. *J. Cell. Physiol.* **229**, 300–308 (2014).

89. Malafoglia, V., Bryant, B., Raffaeli, W., Giordano, A. & Bellipanni, G. The zebrafish as a model for nociception studies. *Journal of Cellular Physiology* **228**, 1956–1966 (2013).

90. Seth, A., Stemple, D. L. & Barroso, I. The emerging use of zebrafish to model metabolic disease. *DMM Disease Models and Mechanisms* **6**, 1080–1088 (2013).

91. Howe, K. *et al.* The zebrafish reference genome sequence and its relationship to the human genome. *Nature* **496**, 498–503 (2013).

92. Bellipanni, G. *et al.* Zebrafish as a Model for the Study of Chaperonopathies. *J. Cell. Physiol.* **231**, 2107–2114 (2016).

93. Tucker, N. R., Middleton, R. C., Le, Q. P. & Shelden, E. A. HSF1 is essential for the resistance of zebrafish eye and brain tissues to hypoxia/reperfusion injury. *PLoS One* **6**, (2011).

94. Burg, L. *et al.* Internal epitope tagging informed by relative lack of sequence conservation. *Sci. Rep.* **6**, (2016).

95. Lawson, N. D. & Wolfe, S. A. Forward and Reverse Genetic Approaches for the Analysis of Vertebrate Development in the Zebrafish. *Developmental Cell* **21**, 48–64 (2011).

96. Van Der Spoel, D. *et al.* GROMACS: Fast, flexible, and free. *Journal of Computational Chemistry* **26**, 1701–1718 (2005).

97. Hess, B., Kutzner, C., Van Der Spoel, D. & Lindahl, E. GRGMACS 4: Algorithms for highly efficient, load-balanced, and scalable molecular simulation. *J. Chem. Theory Comput.* **4**, 435–447 (2008).

98. Foloppe, N. & MacKerell, Jr., A. D. All-atom empirical force field for nucleic acids: I. Parameter optimization based on small molecule and condensed phase macromolecular target data. *J. Comput. Chem.* **21**, 86–104 (2000).

99. MacKerell, A. D. & Banavali, N. K. All-atom empirical force field for nucleic acids: II. Application to molecular dynamics simulations of DNA and RNA in solution. *J. Comput. Chem.* **21**, 105–120 (2000).

100. Bussi, G., Donadio, D. & Parrinello, M. Canonical sampling through velocity rescaling. *J. Chem. Phys.* **126**, (2007).

101. Parrinello, M. & Rahman, A. Polymorphic transitions in single crystals: A new molecular dynamics method. *J. Appl. Phys.* **52**, 7182–7190 (1981).

102. Essmann, U. *et al.* A smooth particle mesh Ewald method. *J. Chem. Phys.* **103**, 8577–8593 (1995).

103. Darden, T., York, D. & Pedersen, L. Particle mesh Ewald: An N·log(N) method for Ewald sums in large systems. *J. Chem. Phys.* **98**, 10089–10092 (1993).

104. Giancarlo, R., Bosco, G. Lo, Pinello, L. & Utro, F. The Three Steps of Clustering In The Post-Genomic Era. in *Biological Knowledge Discovery Handbook* 519–556 (John Wiley & Sons, Inc., 2013). doi:10.1002/9781118617151.ch22

105. Giancarlo, R., Lo Bosco, G. & Utro, F. Bayesian versus data driven model selection for microarray data. *Nat. Comput.* **14**, 393–402 (2015).

106. Camastra, F., Di Taranto, M. D. & Staiano, A. Statistical and Computational Methods for Genetic Diseases: An Overview. *Computational and Mathematical Methods in Medicine* **2015**, (2015).

107. Söderhjelm, P., Tribello, G. A. & Parrinello, M. Locating binding poses in protein-ligand systems using reconnaissance metadynamics. *Proc. Natl. Acad. Sci. U. S. A.* **109**, 5170–5175 (2012).

108. Humphrey, W., Dalke, A. & Schulten, K. VMD: Visual molecular dynamics. *J. Mol. Graph.* **14**, 33–38 (1996).

109. Marino Gammazza, A. *et al.* Elevated blood Hsp60, its structural similarities and cross-reactivity with thyroid molecules, and its presence on the plasma membrane of oncocytes point to the chaperonin as an immunopathogenic factor in Hashimoto's thyroiditis. *Cell Stress Chaperones* **19**, 343–53 (2014).

110. Rappa, F. *et al.* Comparative analysis of hsp10 and hsp90 expression in healthy mucosa and adenocarcinoma of the large bowel. *Anticancer Res.* **34**, 4153–9 (2014).

111. Campanella, C. *et al.* The histone deacetylase inhibitor SAHA induces HSP60 nitration and its extracellular release by exosomal vesicles in human lung-derived carcinoma cells. (2015).

112. Di Felice, V. *et al.* Silk fibroin scaffolds enhance cell commitment of adult rat cardiac progenitor cells. *J. Tissue Eng. Regen. Med.* n/a-n/a (2013). doi:10.1002/term.1739

113. Jao, L. E., Wente, S. R. & Chen, W. Efficient multiplex biallelic zebrafish genome editing using a CRISPR nuclease system. *Proc. Natl. Acad. Sci. U. S. A.* **110**, 13904–13909 (2013).

114. Kalisman, N., Schröder, G. F. & Levitt, M. The crystal structures of the eukaryotic chaperonin CCT reveal its functional partitioning. *Structure* **21**, 540–549 (2013).

115. Willison, K. R. The structure and evolution of eukaryotic chaperonin-containing TCP-1 and its mechanism that folds actin into a protein spring. *Biochem. J.* **475**, 3009–3034 (2018).

116. Melville, M. W., McClellan, A. J., Meyer, A. S., Darveau, A. & Frydman, J. The Hsp70 and TRiC/CCT Chaperone Systems Cooperate In Vivo To Assemble the Von Hippel-Lindau Tumor Suppressor Complex. *Mol. Cell. Biol.* **23**, 3141–3151 (2003).

117. Berger, J. *et al.* In Vivo Function of the Chaperonin TRiC in α-Actin Folding during Sarcomere Assembly. *Cell Rep.* **22**, 313–322 (2018).

118. Minegishi, Y. *et al.* CCT2 mutations evoke leber congenital amaurosis due to chaperone complex instability. *Sci. Rep.* **6**, (2016).

119. Erdmann, J. *et al.* Dysfunctional nitric oxide signalling increases risk of myocardial infarction. *Nature* **504**, 432–436 (2013).

120. Melkani, G. C. *et al.* TRiC/CCT chaperonins are essential for maintaining myofibril organization, cardiac physiological rhythm, and lifespan. *FEBS Lett.* **591**, 3447–3458 (2017).

121. Sot, B. *et al.* The chaperonin CCT inhibits assembly of α-synuclein amyloid fibrils by a specific, conformation-dependent interaction. *Sci. Rep.* **7**, (2017).

122. Tam, S., Geller, R., Spiess, C. & Frydman, J. The chaperonin TRiC controls polyglutamine aggregation and toxicity through subunit-specific interactions. *Nat. Cell Biol.* **8**, 1155–1162 (2006).

123. Behrends, C. *et al.* Chaperonin TRiC Promotes the Assembly of polyQ Expansion Proteins into Nontoxic Oligomers. *Mol. Cell* **23**, 887–897 (2006).

124. Yam, A. Y. *et al.* Defining the TRiC/CCT interactome links chaperonin function to stabilization of newly made proteins with complex topologies. *Nat. Struct. Mol. Biol.* **15**, 1255–1262 (2008).

125. Kasembeli, M. *et al.* Modulation of STAT3 Folding and Function by TRiC/CCT Chaperonin. *PLoS Biol.* **12**, (2014).

126. Moran, A. *et al.* Prevention of trauma/hemorrhagic shock-induced lung apoptosis by IL-6-mediated activation of Stat3. *Clin. Transl. Sci.* **2**, 41–49 (2009).

127. Alten, J. A. *et al.* Prevention of Hypovolemic Circulatory Collapse by IL-6 Activated Stat3. *PLoS One* **3**, e1605 (2008).

128. Trinidad, A. G. *et al.* Interaction of p53 with the CCT Complex Promotes Protein Folding and Wild-Type p53 Activity. *Mol. Cell* **50**, 805–817 (2013).

129. Roh, S. H., Kasembeli, M., Bakthavatsalam, D., Chiu, W. & Tweardy, D. J. Contribution of the type II chaperonin, TRiC/CCT, to oncogenesis. *International Journal of Molecular Sciences* **16**, 26706–26720 (2015).

130. Brown, D. D., Christine, K. S., Showell, C. & Conlon, F. L. Small heat shock protein Hsp27 is required for proper heart tube formation. *Genesis* **45**, 667–678 (2007).

131. Weeks, S. D. *et al.* Characterization of human small heat shock protein HSPB1 α-crystallin domain localized mutants associated with hereditary motor neuron

diseases. *Sci. Rep.* **8**, (2018).

132. The Nervous System by James Follett | Chew The Fat. Available at: http://climatereview.net/ChewTheFat/?attachment_id=1061. (Accessed: 13th November 2019)